

# Anomalous statistics of laser-cooled atoms in dissipative optical lattices

Gadi Afek

*Wright Laboratory,  
Department of Physics,  
Yale University, New Haven,  
Connecticut 06520,  
USA*

Nir Davidson

*Department of Physics of Complex Systems,  
Weizmann Institute of Science, Rehovot 76100,  
Israel*

David A. Kessler and Eli Barkai

*Department of Physics,  
Institute of Nanotechnology and Advanced Materials,  
Bar-Ilan University,  
Ramat-Gan 52900,  
Israel*

(Dated: April 7, 2024)

In this Colloquium we discuss the anomalous kinetics of atoms in dissipative optical lattices, focusing on the “Sisyphus” laser cooling mechanism. The cooling scheme induces a friction force that decreases to zero for high atomic momentum, which in turn leads to unusual statistical features. We study, using a Fokker-Planck equation describing the semi-classical limit of the system, the shallow optical lattice regime where the momentum distribution of the particles is heavy-tailed and the spatial diffusion is anomalous. As the depth of the optical lattice is tuned, transitions in the dynamical properties of the system occur, for example a transition from Gaussian diffusion to a Lévy walk and the breakdown of the Green-Kubo formula for the diffusion constant. Rare events, in both the momentum and spatial distributions, are described by non-normalized states, with tools adapted from infinite ergodic theory. We present experimental observations and elementary explanations for the physical mechanisms of cooling that lead to these anomalous behaviors, comparing theory with available experimental and numerical data.

## CONTENTS

I. Introduction	1	VII. Acknowledgments	20
II. Lévy dynamics and Sisyphus cooling	3	References	20
A. Lévy vs. Gauss central limit theorem, Lévy flights and walks	3		
B. The basics of Sisyphus cooling	5		
III. Anomalous statistics and infinite densities	6		
A. Anomalous dynamics in momentum space	6		
B. From Sisyphus friction to Lévy walks in position space	10		
C. Position-momentum correlations	13		
IV. Implications for fundamental concepts in Statistical Physics	14		
A. Scaling Green-Kubo relation	14		
B. Breakdown of ergodicity	16		
C. Violation of the equipartition theorem	16		
V. Lévy statistics and power-laws in other atomic systems	18		
A. Motional broadening in two-level system ensembles with a heavy-tailed frequency distribution	18		
B. Lévy dynamics in sub-recoil laser cooling	18		
VI. Summary and Conclusions	19		

## I. INTRODUCTION

Laser cooling of atoms is a well-established experimental technique. A momentum-dependent friction force is generated by external optical fields, that tends to reduce the atoms’ velocity towards zero. At the same time, random emissions of photons jolt the atoms, leading to heating and fluctuations of the momentum. The balance between these two mechanisms leads to a steady-state with, potentially, a very narrow momentum distribution. The canonical example is that of Doppler cooling (Phillips, 1998; Wineland *et al.*, 1978). Pairs of counter-propagating beams, red-detuned from the relevant atomic resonance, selectively reduce the momentum of fast-moving atoms. The associated minimal “Doppler” temperature  $T_D$  is given by  $k_B T_D = \hbar \Gamma / 2$ , where  $\Gamma$  is the natural linewidth of the excited state,  $k_B$  is the Boltzmann constant and  $\hbar$  is the reduced Planck con-

stant. This was thought to be a fundamental limit for the ability to laser cool atomic systems. It was, therefore, a great surprise when temperatures below the Doppler limit  $T_D$  were obtained experimentally (Chu, 1998; Cohen-Tannoudji, 1998). The key to explaining this discovery was the multilevel, degenerate nature of atoms. The random momentum recoils  $\hbar k$  due to scattered photons give rise to a second lower bound for the temperature, the recoil limit  $k_B T_R/2 = \hbar^2 k^2/2M = E_R$ , where  $E_R$  is the recoil energy,  $M$  is the atomic mass and  $k$  is the wavenumber. Temperatures even lower than the recoil limit have been achieved through other techniques such as sub-recoil laser cooling (Aspect *et al.*, 1988) and evaporative cooling (Anderson *et al.*, 1995), relying on different physical mechanisms.

The phase-space trajectory of an atom in the semi-classical approximation of the laser cooling mechanism has been analyzed theoretically with tools from quantum optics and the theory of stochastic processes (Dalibard and Cohen-Tannoudji, 1989; Marksteiner *et al.*, 1996). The focus of this Colloquium is the latter. More specifically, we review a stochastic approach to the anomalous dynamics of cold atoms in dissipative lattices and discuss the comparison of its predictions with available numerical and experimental data.

Some intuition can be gained by comparing the motion of the atom in the laser field to diffusion of a small particle in a fluid at room temperature. For such a Brownian particle, in addition to the friction force, a fluctuating force describes the random influence of the surrounding bath. The combined effect of friction and fluctuating force leads to a steady-state of the momentum distribution, namely Maxwell's distribution. The phase-space dynamics can be modelled, under certain approximations, using either the Langevin equation describing the irregular path of the particle or a Fokker-Planck equation for the spatial probability density function. Close to thermal equilibrium, the momentum-momentum correlation function is  $\langle p(t)p(t+\tau) \rangle = Mk_B T \exp(-\gamma\tau)$ . The fact that the correlation function does not depend on  $t$  means that the process is stationary and the correlation function decays exponentially with a damping constant  $\gamma$ . A packet of such particles starting from a common origin and spreading for duration  $t$  is described by a Gaussian distribution, as is expected from the central limit theorem, with a mean squared displacement (MSD) of  $\langle x^2 \rangle = 2Dt$  where  $D$  is the diffusion constant. Using  $x(t) = \int_0^t dt' p(t')/M$  and the fact that the process is stationary, the Green-Kubo relation (Green, 1954; Kubo, 1957),  $D = \frac{1}{M^2} \int_0^\infty d\tau \langle p(\tau)p(0) \rangle$  can be derived. Plugging in the exponentially decaying correlation function gives the famous Einstein relation  $D = k_B T/M\gamma$  (Einstein, 1905), relating the strength of the fluctuating force  $D$ , the dissipation  $\gamma$  and the temperature  $T$ . The system discussed in this Colloquium exhibits a breakdown of all of these standard relations.

The specific physical mechanism at hand is called *Sisyphus cooling* or *polarization gradient cooling*. It is implemented experimentally using a pair of red-detuned, counter-propagating laser-beams of orthogonal polarization, creating an optical lattice with spatially varying polarization along the beam axis. The lattice has a modulation depth  $U_0$  describing the amplitude of the spatial oscillations of the potential minima felt by the atoms, whose ratio with the recoil energy plays a crucial role in the description of the dynamics (Sec. II.B). Optimal cooling is found for a certain value of this ratio, and at the same time two surprising phenomena are observed when it is varied. The diffusion constant  $D$  describing the transport was predicted to diverge at a critical value of  $U_0/E_R$ , associated with a failure of the widely-used Green-Kubo formalism. This divergence was indeed experimentally observed as a dramatic increase in the diffusivity (Hodapp *et al.*, 1995). Other early experiments investigated the average kinetic energy of the atoms and, upon loading them into a harmonic trap, their mean potential energy (Katori *et al.*, 1997). A sharp increase of these observables was witnessed, corresponding to a transition from a deep to a shallow lattice regime (Sec. III). These findings can be explained using a semi-classical treatment of the atom-laser system and a Fokker-Planck equation introduced in (Dalibard and Cohen-Tannoudji, 1985), and are closely related to the heavy power-law tails of the steady-state momentum probability density (Douglas *et al.*, 2006).

These transitions result from a peculiar feature of the system's damping mechanism, described in detail in Sec. II.B. For large momentum the friction force  $f \sim -1/p$ , decreases as the momentum increases, rendering the system practically dissipationless for fast-moving atoms. This is in contrast to the small  $p$  behavior  $f \sim -p$ , which provides highly efficient damping. An atom that happens to experience a large fluctuation giving it a large momentum will experience very little friction and will instead have to depend on the fluctuations to drive it back to the cold state. The steady-state momentum distribution is now described by power-law statistics instead of the familiar Maxwell distribution, and in turn the spatial spreading of the particle density exhibits anomalous, Lévy-type diffusion. The divergence of the diffusion constant implies the onset of super-diffusion, namely the MSD  $\langle x^2 \rangle \sim t^\beta$  with  $\beta > 1$ , in contrast to the normal diffusion case for which  $\beta = 1$ .

In general, mechanisms leading to anomalous diffusion have been well-investigated (especially the stochastic aspects of the problem), leading to concepts like Lévy flights and Lévy walks (Bouchaud and Georges, 1990; Metzler *et al.*, 2014; Metzler and Klafter, 2000; Zaburdaev *et al.*, 2015). The ability to precisely tune the control parameters, and hence the ensuing anomaly, is a unique advantage of atomic systems. It is not common that a basic theory such as that of Sisyphus cooling can

lead to a detailed theoretical understanding of the origins of anomalous diffusion, usually found in truly complex settings such as biological systems (Barkai *et al.*, 2012; Levin *et al.*, 2021; Lo *et al.*, 2002), economics (Plerou *et al.*, 2000) or turbulent flows (Richardson, 1926). Furthermore, these atomic systems enable both one-shot ensemble averaging of millions of particles, single-particle tracking (Bouton *et al.*, 2020; Katori *et al.*, 1997; Kinermann *et al.*, 2016) and the application of advanced spectral analysis tools. This makes them unique as a model system for testing statistical physics in general, including the study of such basic concepts as the Clausius inequality (Mayer *et al.*, 2020) and the Caldeira-Leggett model (Mulder *et al.*, 2021), and anomalous dynamics in particular.

These anomalous statistics create many interesting challenges, some of which were briefly discussed in a previous review (Lutz and Renzoni, 2013). For example, given that the Green-Kubo formalism fails, what is the theoretical framework which enables the calculation of the super-diffusion effect? Also, the steady-state theory predicts that the energy should diverge, an unphysical conclusion, and hence some cutoff must naturally arise in the steady-state description. This can stem in principle from new physical effects, however here we promote the concept of infinite densities (Akimoto, 2008; Korabel and Barkai, 2009) which treats correctly the rare fluctuations of the system and their essential dependence on time, and so removes divergences found in the steady-state theory. Equally importantly, it relates the dynamics of the cold atoms to a branch of pure mathematics called infinite ergodic theory (Aaronson, 1997). It is therefore evident that the very basic concepts of equilibrium statistical physics, transport theory and even the fundamental theory of gases must be treated with extra care when applied to these systems.

The focus of this Colloquium is on the statistical and experimental aspects of the problem, while the mechanism of laser cooling is only covered briefly. It is our hope that this presentation will expose the present state of the theory, its comparison to available experimental data, and trigger further investigation in the field.

## II. LÉVY DYNAMICS AND SISYPHUS COOLING

### A. Lévy vs. Gauss central limit theorem, Lévy flights and walks

The process of Brownian motion was modelled by Einstein, Smoluchowski and others (Hänggi and Marchesoni, 2005; Kubo, 1957; Li and Raizen, 2013; Majumdar, 2007). The spreading in one-dimension (1d) of an ensemble of such particles, all starting from a common origin is characterized by a MSD that grows linearly with time,  $\langle x^2 \rangle \sim t$ . It is very natural that the underlying random

walk process describing Brownian motion is Gaussian as this is precisely what the central limit theorem predicts, as the total displacement at long times is a sum of many independent random displacements. However, starting with the work of Richardson (Richardson, 1926), who showed that the relative separation of weather balloons in the turbulent atmosphere is described by  $\langle x^2 \rangle \sim t^3$ , both mathematicians and physicists have been searching for extensions to the basic laws of diffusive processes.

One very successful theory parametrizing the deviation from normal, Gaussian, Brownian motion is that of the random walk governed by Lévy laws. The differences between such scale-free processes and normal ones are highlighted below, following a brief introduction to Lévy statistics (Amir, 2020), a generalization of the standard central limit theorem. Central limit theorems deal with the problem of summation of a large number  $N$  of independent, identically-distributed (IID) random variables  $\{\chi_i\}$ . The sum  $S = \sum_{i=1}^N \chi_i / N^{1/\mu}$ , scaled by some power  $1/\mu$  of  $N$  is considered. The probability density function (PDF) of  $S$  is given by the inverse Fourier transform of its characteristic function,

$$\begin{aligned} \langle \exp(ikS) \rangle &= \left\langle \exp\left(\frac{ik\chi_1}{N^{1/\mu}}\right) \right\rangle \cdots \left\langle \exp\left(\frac{ik\chi_N}{N^{1/\mu}}\right) \right\rangle \\ &= \left\langle \exp\left(\frac{ik\chi}{N^{1/\mu}}\right) \right\rangle^N. \end{aligned} \quad (1)$$

The result is a direct outcome of the assumption that the random variables  $\{\chi_i\}$  are IID and so the expectation value factorizes. We will assume that the PDF of the summand  $\chi$  is symmetric so its mean is zero. Two examples are a Gaussian PDF, with standard deviation  $\sigma$ ,  $P_G(\chi) = \exp(-\chi^2/2\sigma^2)/\sqrt{2\pi\sigma^2}$  and a Lorentzian  $P_L(\chi) = [\pi(1 + \chi^2)]^{-1}$ . The first is an example of a distribution with finite moments. The second has a power-law tail, and its variance diverges. The characteristic function of the Gaussian is  $\tilde{P}_G(k) = \exp(-k^2\sigma^2/2)$ , while for the Lorentzian  $\tilde{P}_L(k) = \exp(-|k|)$ . Related to the divergence of the variance, the characteristic function of the Lorentzian exhibits non-analytical behavior at  $k = 0$ ,  $P_L(k) \sim 1 - |k|$  and the second derivative with respect to  $k$  at this point diverges. More generally, if  $P(\chi) \sim |\chi|^{-(1+\nu)}$  for large  $|\chi|$  and  $0 < \nu < 2$ , then for small  $k$  we have  $\tilde{P}(k) \sim 1 - A|k|^\nu$ , where  $A$  is a scale parameter. The choice  $\nu < 2$  implies that the variance of the summand diverges. On the other hand, for any parent distribution of the summand with a finite variance, we have  $P(k) \sim 1 - \sigma^2 k^2/2$  where the leading term reflects the fact that  $P(\chi)$  is normalized. Then, using Eq. 1, two generic possibilities are found in the limit of  $N \rightarrow \infty$ . If the variance of  $P(\chi)$  is finite,

$$\langle \exp(ikS) \rangle \rightarrow \left(1 - \frac{\sigma^2 k^2}{2N}\right)^N = \exp(-\sigma^2 k^2/2) \quad (2)$$

where we choose  $\mu = 2$  and use the definition of the exponential limit. This implies a diffusive scaling for the sum. Importantly, it also means that the PDF of the scaled sum  $S$  is Gaussian for *any* parent distribution with a finite variance. In contrast, if  $P(\chi)$  exhibits power-law decay, and  $\mu$  is chosen such that  $\mu = \nu$ ,

$$\langle \exp(ikS) \rangle \rightarrow \left(1 - \frac{A|k|^\nu}{N}\right)^N = \exp(-A|k|^\nu). \quad (3)$$

The choice  $\nu < 2$  implies  $\mu < 2$  and super-diffusive scaling, as the sum of the random variables grows like  $N^{1/\mu}$ . To summarize, the sum of random variables is scaled with  $N^{1/\mu}$ . If  $\nu > 2$  (so that the variance exists) then  $\mu = 2$ , while if  $\nu < 2$  (and the variance diverges) then  $\mu = \nu$ . The inverse Fourier transform of Eq. 3 is the PDF of the sum  $S$  and is also the well-known symmetric stable density or Lévy density (Amir, 2020; Bouchaud and Georges, 1990)-

$$L_{\nu,0}(S) = \frac{1}{2\pi} \int_{-\infty}^{\infty} dk \exp(ikS - |k|^\nu), \quad (4)$$

where the subscript 0 indicates symmetric functions and the width scale is set to 1. The case  $\nu = 1$  is the Lorentzian and  $\nu = 2$  the Gaussian. There now emerge two forms of central limit theorems, usually associated with Gauss (Eq. 2) and Lévy (Eq. 3). When a system exhibits power-law statistics of the Lévy type, the largest summand in the set  $\{\chi_i\}$  is of the order of the sum, with one term dominating the entire sum (Chistyakov, 1964; Vezzani *et al.*, 2019). The fact that the variance diverges and the mean is zero implies a random fractal, also called a “self-similar” object, easily visualised considering a 2d Lévy flight, as depicted in Fig. 1.

Specific examples of Lévy stable densities emerged in physics, absent the general framework of the mathematicians, in the context of the summation of a large number of forces or energies already more than a century ago. In his line-shape theory, Holtsmark (Holtsmark, 1919) considered the sum of many perturbations acting on an ion, and a similar problem was later considered by Chandrasekhar (Chandrasekhar, 1943) in an astrophysical context. The Holtsmark distribution is a particular, yet significant case of the Lévy stable distribution, with  $\nu = d/n$ , where  $d = 3$  is the dimension of the system and  $n = 2$  is the power of the spatial dependence of the interaction potential, *i.e.* gravitational or Coulomb. It applies when considering the projected force on one of the axes and when the bath particles are uniformly distributed in space. Landau, in his work on the energy transfer due to multiple scatterings in ionization, constructed what would become known as the one-sided Lévy stable distribution (Landau, 1944). Similar ideas and behaviors are found for single molecules in low tem-

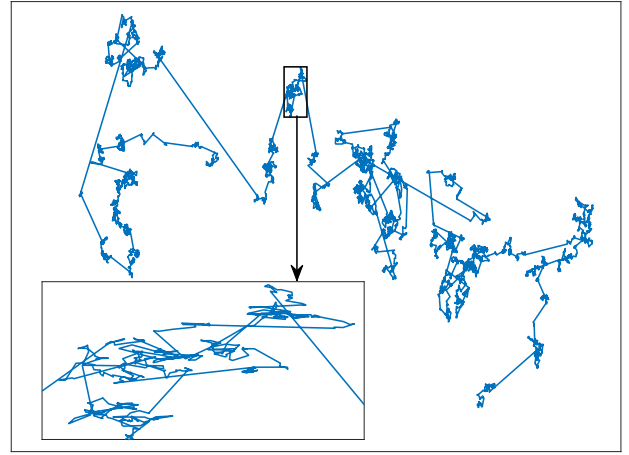


FIG. 1 Lévy flights are random walk processes where the jump lengths are obtained from heavy-tailed power-law distributions with infinite variance (Eq. 3). Depicted is an example of a two-dimensional Lévy flight with  $\nu = 1.4$ , where the jump angle is uniformly distributed. The fractal nature of the dynamics is evident from the inset, similarly characterized by a small number of long flights and a large number of short flights.

perature glasses (Barkai *et al.*, 2003, 2000), and models of active dynamics (Kanazawa *et al.*, 2020). Lévy stable densities emerged in physics from widely applicable and simple long-range interacting models, and we can now understand the many results in this field as a manifestation of the mathematics developed by Lévy and others.

A random walk can be viewed as a sum of IID random variables, with each summand representing the length of a jump and  $N$  representing a discrete time. Indeed, Brownian motion, which is a continuum description of a random walk, is a Gaussian process for all time intervals. The concept of a Lévy flight, where either scalar or vector displacements are drawn from a common PDF with a power-law tail and summed, is therefore appealing. This is, however, clearly problematic for a process describing spatial dynamics, as larger steps in space are expected to take longer. The power-law tail of the distribution of the size of the jumps means that the MSD of the Lévy flight is infinite, which is unphysical as any real system will have a maximal speed of propagation. To remedy this, the concept of Lévy walks was introduced by (Shlesinger *et al.*, 1987; Zaburdaev *et al.*, 2015).

The simplest, 1d version of the Lévy walk, considers a particle starting at the origin at  $t = 0$ . A random walk duration  $\tau$  is drawn from the long-tailed PDF  $\psi(\tau)$ . A random velocity is also drawn, for example  $\pm V_0$  with probability 1/2. During this interval the motion is ballistic, reaching  $x = V_0\tau$ . The process is then repeated (“renewed”) and a new pair of walk duration and velocity is drawn. The position  $x(t)$  of the particle is limited by the ballistic light cone  $-V_0t < x(t) < V_0t$ , and the moments



of  $x(t)$  never diverge. If the distribution of walk durations does not have power-law tails, but is exponential, this model is essentially the Drude model for transport of electrons in metals and the diffusion is normal. In the Lévy walk case, the walk duration PDF is heavy tailed,  $\psi(\tau) \sim \tau^{-(1+\eta)}$ . Here, if  $0 < \eta < 1$  the mean flight duration diverges, while if  $1 < \eta < 2$  the variance of the flight duration diverges. Below we relate the exponents  $\eta$ , describing the waiting times,  $\mu$ , the rescaling of the sum and  $\nu$ , the heavy-tail exponent of the PDF of the summand, to the parameters of the optical lattice (Eq. 21). This yields three dynamical phases for the MSD (Zaburdaev *et al.*, 2015)

$$\langle x^2(t) \rangle \sim \begin{cases} t^2 & 0 < \eta < 1 \\ t^{3-\eta} & 1 < \eta < 2 \\ t & \eta > 2. \end{cases} \quad (5)$$

When  $\eta < 1$  the dynamics are ballistic, whereas for  $1 < \eta < 2$  the spreading is super-diffusive. When the first two moments of the PDF of the travel duration are finite ( $\eta > 2$ ), normal diffusion is recovered. In the Lévy walk, therefore, by introducing the finite velocity, a natural cutoff is created, curing the unphysical divergence of the variance of displacement in the corresponding Lévy flight. Another major difference between Lévy walks and Lévy flights is that in the latter the number of steps  $N$  is fixed, like in any other random walk process, whereas in the Lévy walk the number of renewals in the time interval  $(0, t)$  is itself a random variable (Godreche and Luck, 2001).

There are many physical applications of Lévy walks. For example, blinking quantum dots (Brokmann *et al.*, 2003; Margolin and Barkai, 2005; Stefani *et al.*, 2009) work in the ballistic phase  $0 < \eta < 1$ , where the effective velocity is actually the intensity of emitted light which jumps between dark and bright states, with power-law distributed sojourn times. The position of the random walker corresponds to the total number of photon counts which exhibits super-diffusive statistics, as seen in the laboratory (Margolin *et al.*, 2006). Lévy walks appear also in the motion of bacterial colonies (Ariel *et al.*, 2015), and in many other applications (Zaburdaev *et al.*, 2015).

## B. The basics of Sisyphus cooling

The mechanism by which anomalous diffusion is manifested within the context of cold atomic ensembles in dissipative optical lattices, is related to the nonlinear nature of the momentum-dependent optical friction force  $f(p)$  acting on the atoms (Agarwal and Molmer, 1993; Castin *et al.*, 1991; Castin and Molmer, 1990; Dalibard and Cohen-Tannoudji, 1989; Marksteiner *et al.*, 1996). It is unique in that the friction vanishes for fast atoms. In

the semi-classical approximation, it takes the form

$$f(p) = -\frac{\mathcal{A}p}{1 + (p/p_c)^2}. \quad (6)$$

The strength of the friction force  $\mathcal{A}$  and the momentum capture range  $p_c$  depend on  $U_0$  through the chosen set of experimental parameters, namely the detuning  $\delta$  from the atomic resonance and the intensity of the beams (Castin *et al.*, 1991). A slow atom with  $p/p_c \ll 1$  will experience a drag-like force  $f \sim -p$  similar to the Stokes friction acting on a Brownian particle in fluid, whereas a fast atom feels a force  $f \sim -1/p$ . Intuitively, fast-moving atoms tend to remain fast, leading to large flights in space and in turn to anomalous, Lévy-type motion.

The friction force can be rigorously derived in the semi-classical limit together with the noise in the system, relying on the generic model of laser cooling in the  $J = 1/2$  to  $J' = 3/2$  atomic transition (Fig. 2). The full derivation of the mechanism extends beyond the scope of this Colloquium, and instead we present a simplified physical picture, based on a consideration of the average energy loss, that yields the effective friction force. The Sisyphus effect is based on the transfer of population between the different sub-levels of the ground-state manifold of atoms (optical pumping via the excited states) as they move through a specifically configured light field (Castin *et al.*, 1991; Castin and Molmer, 1990; Dalibard and Cohen-Tannoudji, 1989). As an atom moves through the optical lattice, it has a higher probability to absorb a photon when it is in the upper ground state level ( $J = 1/2, m = \pm 1/2$ , the sign depending on the position in the lattice) and then decay to the lower ground state ( $J = 1/2, m = \mp 1/2$ ), resulting in a net energy loss of  $U_0$  (Fig. 2). This is reminiscent of the Greek myth of Sisyphus, doomed to repeatedly roll a boulder up a mountain. Climbing the potential hill changes the momentum of the atom from  $p$  to  $p + \delta p$ , where energy conservation dictates  $p^2/(2M) - U_0 = (p + \delta p)^2/(2M)$ . For large  $p$ , linearization yields  $\delta p \simeq -U_0 M/p$ . The minus sign means that the atom, on average, slows down. This process repeats at some rate  $\tilde{\Gamma}$  yielding an effective friction force  $f \simeq \tilde{\Gamma} \delta p \simeq -\tilde{\Gamma} U_0 M/p$ . A detailed calculation gives  $f \simeq -\Gamma s_0 U_0 M/p$  where  $\Gamma s_0$  is the product of the inverse life time of the excited state and the saturation  $s_0$  which is a measure of occupancy in the excited state.

To realize this friction (Chu, 1998; Cohen-Tannoudji, 1998), consider an atom that has a lower energy level with angular momentum  $J = 1/2$  and an upper energy level with  $J' = 3/2$  that moves through a standing wave formed by two counter-propagating laser beams with orthogonal linear polarization, also known as the lin  $\perp$  lin configuration (Fig. 2). The resulting polarization depends on the relative phase of the two laser beams and varies periodically with position. This polarization gradi-

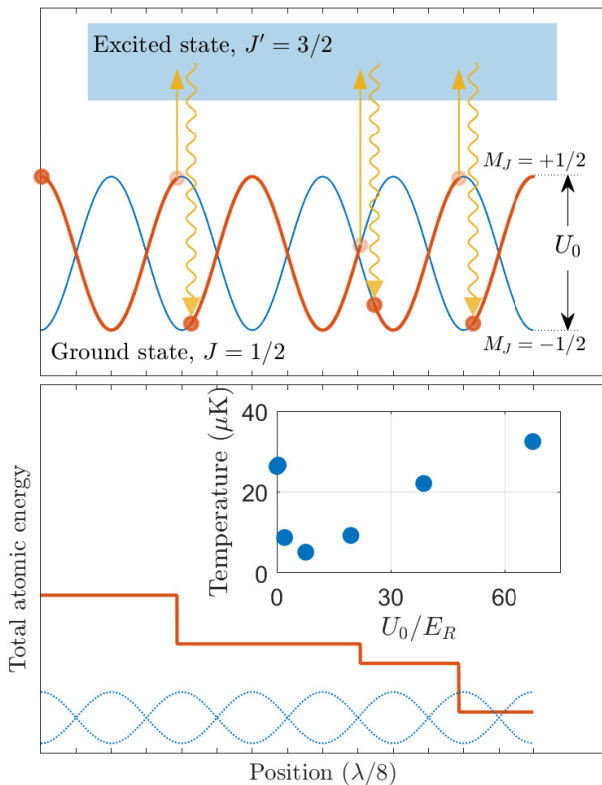


FIG. 2 Adapted from (Castin *et al.*, 1991). L  vy dynamics can arise in the motion of ultracold atoms undergoing *Sisyphus cooling*. Two counter-propagating, orthogonally-linearly-polarized laser beams generate a periodic spatial modulation of the polarization. The atomic energy levels are then periodically perturbed by the light, so that the atom travels up and down hills and valleys (top). Kinetic energy is dissipated when the atom absorbs a photon at the upper part of a hill and spontaneously emits a photon of higher frequency, ending up in a valley. This can be made more probable than the reverse process, so that effectively there is a strong cooling effect (bottom). Atoms in this standing wave are thus cooled below the Doppler limit. The main control parameter is the modulation-depth of the lattice  $U_0$  (Eq. 7). The inset shows a measurement of the temperature, proportional to the mean kinetic energy, of  $^{87}\text{Rb}$  atoms subjected to Sisyphus cooling at different lattice depths (Afek and Davidson, 2018).

ent causes periodic modulation of the states in the lower level manifold due to Stark shifts. In this cleverly engineered optical lattice, the probability of the downhill transitions is enhanced when the particle is at the top of the potential. The calculation involves the transition probabilities as a function of position due to the optically modulated fields, and then averaging over the spatial period of the optical lattice. Sisyphus cooling reaches a non-equilibrium steady-state, where the friction force that biases the system to zero momentum is balanced with the fluctuations caused by spontaneous emission. For large values of potential depth  $U_0$  (“deep” lattices) the effective

temperature (*i.e.* the mean kinetic energy  $\langle E_k \rangle$ ) is proportional to and of the order of  $U_0$  (Cohen-Tannoudji, 1998). This can be understood given that once the energy of the atom is smaller than  $U_0$  it cannot climb up the hill, and hence at this stage cooling is ineffective. As  $U_0$  is reduced the effective temperature reaches a minimum at some  $U_0^{\min}$  and then rises sharply upon further reduction of  $U_0$  (“shallow” lattices). At this minimum,  $\langle E_k \rangle \sim U_0^{\min}$  (see inset of Fig. 2 where the minimal temperature is obtained at  $U_0^{\min}/E_R \approx 10$ ). The distinction between shallow ( $U_0 < U_0^{\min}$ ) vs. deep ( $U_0 > U_0^{\min}$ ) lattices, that will be shown to mark the transition between different regimes in the dynamics, then follows naturally.

$U_0$  is hence an important control parameter in this problem, and a useful dimensionless form of it can then be defined as

$$\tilde{U}_0 = \frac{1}{C} \frac{U_0}{E_R} = \frac{1}{C} \frac{M\delta s_0}{\hbar k^2}. \quad (7)$$

Different values are cited in the literature for  $C$ , reflecting the complexity of experimental atomic systems beyond the simplified models (Castin and Molmer, 1990; Marksteiner *et al.*, 1996). However, the numerical value does not have a profound affect on the results presented here, and therefore it is reasonable to treat  $C$  as a dimensionless fitting parameter.

### III. ANOMALOUS STATISTICS AND INFINITE DENSITIES

#### A. Anomalous dynamics in momentum space

We now turn to a quantitative description of the anomalous dynamics of the momentum distribution. For 1d motion in the dissipative lattice, after averaging over the lattice period and using the semiclassical approximation, it has been shown (Castin *et al.*, 1991; Hodapp *et al.*, 1995; Lutz, 2004) that the dynamics of the momentum PDF  $W(p, t)$  is governed by the following Fokker-Planck equation

$$\frac{\partial W}{\partial t} = -\frac{\partial}{\partial p} [f(p)W] + \frac{\partial}{\partial p} \left[ D(p) \frac{\partial W}{\partial p} \right], \quad (8)$$

valid for shallow lattices. In the opposite limit of deep lattices, the spatial structure of the lattice and the energy surfaces play an important role and cannot simply be averaged out. The diffusive term  $D(p) = D_0 + D_1/[1 + (p/p_c)^2]$  describes stochastic fluctuations of the momentum, which in the absence of friction lead to heating.  $D_0$  and  $D_1$  are functions of the experimental parameters (Castin and Molmer, 1990; Marksteiner *et al.*, 1996). Unlike the friction force that vanishes in the limit of large momentum, the momentum diffusion becomes  $p$ -independent in this limit, and  $D(p) \rightarrow D_0$ . The simple

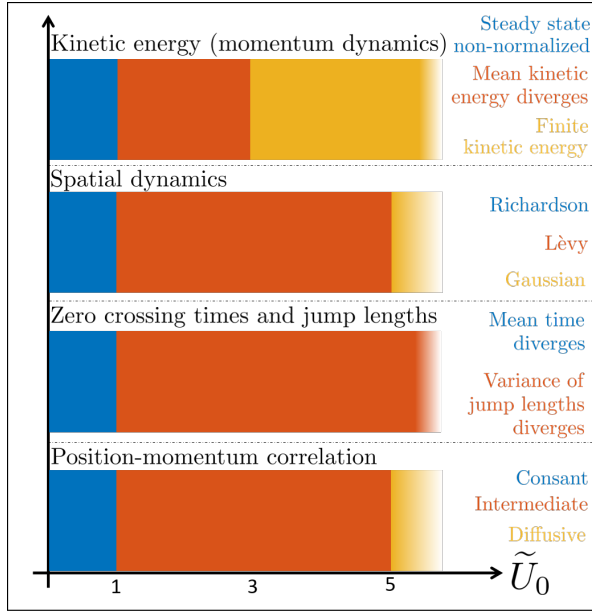


FIG. 3  $\tilde{U}_0$ , defined in Eq. 7 and Fig. 2, is the modulation-depth of the optical lattice, scaled by the recoil energy  $E_R$ . It controls the statistical properties of the system and can be varied using conveniently controlled experimental knobs such as the power of the cooling laser and its detuning from the relevant atomic resonance. Momentum, position and position-momentum correlation all display sharp transitions between different regimes as it is scanned. See Eqns. 19 (Sec. III.A), 21, 23 (Sec. III.B) and 25 (Sec. III.C) for details. Unphysical divergences are resolved when moments are calculated using the formalism of the *infinite covariant density*.

relation between friction and dissipation, in the spirit of the Einstein relation, is hence invalid.

The steady-state solution of Eq. 8,  $W(p)$ , was derived in (Lutz, 2003). Using the force given by Eq. 6 and the diffusive term discussed above, it reads

$$W(p) \sim \left[ 1 + \frac{D_0}{D_0 + D_1} \left( \frac{p}{p_c} \right)^2 \right]^{-\tilde{U}_0/2}. \quad (9)$$

The width of the momentum distribution is determined by  $p_c$ , and it has a power-law heavy tail with an exponent that can be expressed in terms of  $\tilde{U}_0$  as  $W(p) \sim |p|^{-\tilde{U}_0}$ . The second moment of the steady-state momentum  $\langle p^2 \rangle = \int_{-\infty}^{\infty} dp p^2 W(p)$ , usually considered as a measure of the temperature, diverges when  $\tilde{U}_0 < 3$ . Moreover, when  $\tilde{U}_0 < 1$  the solution is itself no longer normalizable and there is no steady-state. Fig. 3 schematically presents the three phases of the dynamics in momentum space. It also shows the dynamical transition found in real space, zero-crossing times and jump lengths (based on a Langevin picture soon to be introduced) and position-momentum correlation, treated in Sec. III.B and III.C. The experimental verification of Eq. 9 was pre-

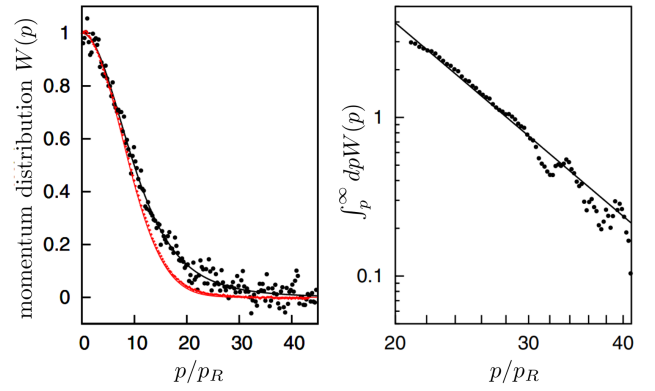


FIG. 4 Adapted from (Douglas *et al.*, 2006). Analysis of the atomic dynamics under the unique Sisyphus friction (Eq. 6) predicts a non-Gaussian steady-state in momentum (Eq. 9). The left panel shows the results of a time-of-flight measurement of the momentum distribution  $W(p)$  of an ensemble of Cs atoms vs. momentum, rescaled by the recoil momentum  $p_R = \sqrt{2ME_R}$ , in a deep lattice (red markers, almost coinciding with red line) and a shallow lattice (black points). Solid lines represent fits to Eq. 9, giving a Gaussian distribution for the deep lattice (red) and a power-law for the shallow lattice (black). (right) Integrated data from the left panel, plotted on a log-log scale, revealing the power-law nature of the distribution.

sented in (Douglas *et al.*, 2006). Fig. 4 shows data from a time-of-flight measurement of the momentum distribution of an ensemble of Cs atoms in a 3d dissipative lattice, demonstrating the power-law nature of the distribution.

*Langevin picture.* In analyzing the dynamics described in Eq. 8, it is convenient to also consider the corresponding Langevin equation describing the phase space trajectory of a particle. These are Newton's laws in the presence of friction and noise. The analysis of paths is extremely useful for a myriad of reasons, ranging from ease of simulations that allow insight on individual trajectories, to more advanced properties of the system such as the analysis of time averages to tackle issues like ergodicity (discussed in Sec. IV.B).

For simplicity, we set  $D_1 = 0$ , since it modifies neither the asymptotic  $|p| \rightarrow \infty$  behavior of the heating term nor the cooling force, and therefore does not affect the main conclusions. Transforming to dimensionless time  $t \rightarrow \mathcal{A}t$ , momentum  $p \rightarrow p/p_c$  and position  $x \rightarrow xMA/p_c$ , the Langevin equation, with  $\xi(t)$  being white Gaussian noise with zero mean and unit strength, reads

$$\frac{dp}{dt} = f(p) + \sqrt{2/\tilde{U}_0} \xi(t); \quad \frac{dx}{dt} = p, \quad (10)$$

where the dimensionless form of the force of Eq. 6 now reads  $f(p) = -p/(1 + p^2)$ .

Returning to the non-normalizability of the steady

state for  $\tilde{U}_0 < 1$  points to a dynamical transition. The time it takes a particle with momentum  $p > 0$  to cross zero is random, and as discussed in Sec. III.B, the PDF of these times is described by a power-law,  $\psi(\tau) \sim \tau^{-(1+\eta)}$ , with  $0 < \eta \leq 1$  for  $\tilde{U}_0 \leq 1$ . The non-normalised steady-state is thus related to the divergence of the mean return time. To analyse these topics, a description in terms of paths is needed, based on the Langevin picture. Even though the energy cannot realistically diverge, measurements of ensemble averaged kinetic energy  $\langle p^2 \rangle / 2M$  do exhibit a sharp transition at a certain  $\tilde{U}_0$ , below which the energy increases dramatically (Fig. 2, inset).

Two theoretical challenges now arise. First, is the Fokker-Planck description generally valid? To address this, one typically resorts to experiments, numerical simulations of the underlying master equation or quantum Monte Carlo simulations. Secondly, assuming the Fokker-Planck equation is valid, is the associated steady-state  $W(p)$  a valid description over times which are long but finite? In fact, the steady-state by itself does not yield a complete description of the momentum distribution. In particular, all moments of the momentum distribution as specified by the time-dependent Fokker-Planck equation are finite for any finite measurement time, in contrast to the steady-state prediction made based on Eq. 9. To obtain these moments, including the second moment (which gives the ensemble-averaged kinetic energy) for  $\tilde{U}_0 < 3$ , a new tool is needed called the *infinite covariant density*.

*Infinite covariant density.* The steady-state momentum distribution in this dimensionless form, corresponding to Eq. 9, reduces to

$$W(p) = \mathcal{N}(1 + p^2)^{-\tilde{U}_0/2} \quad \text{for } \tilde{U}_0 > 1 \quad (11)$$

with  $\mathcal{N} = \Gamma(\tilde{U}_0/2) / [\sqrt{\pi}\Gamma(\frac{\tilde{U}_0-1}{2})]$ . Here  $\Gamma$  is the Gamma function. As mentioned above, for  $\tilde{U}_0 \leq 1$  the solution is no longer normalizable. For  $\tilde{U}_0 > 1$ , the steady-state second moment is

$$\langle p^2 \rangle = \begin{cases} \frac{1}{\tilde{U}_0-3} & \text{for } \tilde{U}_0 > 3 \\ \infty & \text{for } \tilde{U}_0 < 3. \end{cases} \quad (12)$$

This divergence of the steady-state kinetic energy  $\langle p^2 \rangle$  as  $\tilde{U}_0$  approaches its critical value of 3 from above is the direct result of the power-law tail of the momentum distribution, which in turn is due to the weak friction force at large momentum  $f(p) \sim -1/p$ . The key insight here is that, for these types of systems, the difference between the steady-state distribution and the distribution at a large but finite time is non-negligible, in contradiction to what happens for the standard  $f(p) \sim -p$  friction force. While the bulk of the distribution is given correctly by

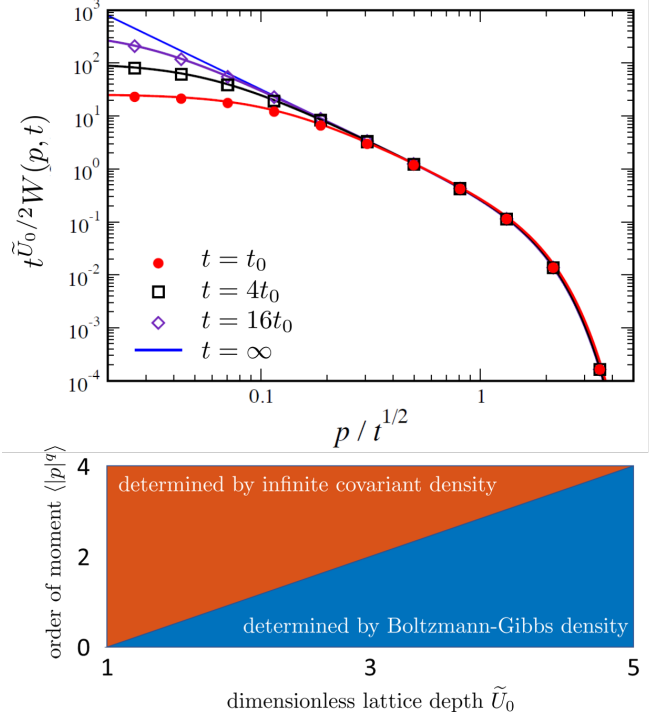


FIG. 5 (top) Adapted from (Kessler and Barkai, 2010). Temporal dynamics of the momentum distribution. The rescaled density of momentum versus  $p/t^{1/2}$  obtained from Langevin simulations (dimensionless units, Eq. 10) with  $\tilde{U}_0 = 2$  for rescaled times  $t = t_0 \equiv 76.3$ ,  $t = 4t_0$  and  $t = 16t_0$ , emphasizing the large momentum of the atom where the scaling is effectively diffusive as the friction is small. The theoretical curve is the *infinite covariant density* of Eq. (16) which is a valid description in the long time limit. It exhibits a Gaussian-like cutoff of the momentum distribution, which renders the moments finite, unlike those of the formal steady-state. The area under the curve diverges when  $t \rightarrow \infty$ , related to the power-law blow up at small momentum. This small  $p$  power-law divergence in the infinite covariant density matches the large  $p$  decay of the steady state PDF of Eq. 11 (bottom) Adapted from (Holz et al., 2015).  $q^{\text{th}}$  moment of the momentum vs. lattice depth  $\tilde{U}_0$ , showing the complementarity of the two densities in calculating moments of the observables. The steady state is termed “Boltzmann-Gibbs” since it describes an effective motion in a logarithmic potential (see text).

the steady-state solution, the power-law tail of the time-dependent  $W(p, t)$  does not extend to infinite momentum. Just as in the case of free diffusion in momentum space, where the momentum very rarely exceeds  $\sim \sqrt{t}$ , so too here the power-law tail is cuff off at  $p \sim \sqrt{t}$ . To see this, a careful analysis of the dimensionless Fokker-Planck equation

$$\frac{\partial W}{\partial t} = \left( \frac{1}{\tilde{U}_0} \frac{\partial^2}{\partial p^2} + \frac{\partial}{\partial p} \frac{p}{1 + p^2} \right) W \quad (13)$$

was presented in (Dechant et al., 2011a; Kessler and Barkai, 2010; Levine et al., 2005), employing the scaling



ansatz

$$W(p, t) \sim t^q h(p/\sqrt{t}) \quad (14)$$

which holds for large momentum and long time. Using the diffusive scaling variable  $z = p/\sqrt{t}$ , one then finds the following equation

$$\frac{1}{\tilde{U}_0} \frac{d^2 h}{dz^2} + \left( \frac{1}{z} + \frac{z}{2} \right) \frac{dh}{dz} - \left( q + \frac{1}{z^2} \right) h = 0. \quad (15)$$

Matching this solution to the steady-state solution which holds for  $p \ll \sqrt{t}$  gives  $q = -\tilde{U}_0/2$ , and

$$h(z) = \frac{\mathcal{N} z^{-\tilde{U}_0}}{\Gamma\left(\frac{\tilde{U}_0+1}{2}\right)} \Gamma\left(\frac{1+\tilde{U}_0}{2}, \frac{\tilde{U}_0 z^2}{4}\right) \quad (16)$$

where  $\Gamma(a, x)$  is the incomplete Gamma function. In the small and large  $z$  limits,

$$h(z) \sim \begin{cases} \mathcal{N} z^{-\tilde{U}_0} & z \ll 2/\sqrt{\tilde{U}_0} \\ \frac{\mathcal{N}(4/\tilde{U}_0)^{(1-\tilde{U}_0)/2}}{\Gamma[(\tilde{U}_0+1)/2]} z^{-1} e^{-\tilde{U}_0 z^2/4} & z \gg 2/\sqrt{\tilde{U}_0}. \end{cases} \quad (17)$$

The Gaussian factor found for large  $z$  stems from diffusion in momentum space, as the force becomes negligible for large momentum, and indeed cuts  $W$  off for  $p \gg \sqrt{t}$ . The small- $z$  behavior is a power-law that matches the large- $p$  behavior of the steady-state of Eq. 11.

The solution  $h(z)$  is non-normalizable, since  $h(z) \sim z^{-\tilde{U}_0}$  for small  $z$ . This type of solution is called an infinite covariant density. It is *covariant* in the sense that  $z = p/\sqrt{t}$ , hence  $p$  must be scaled with the square root of time [namely  $h(z)$  remains fixed as both  $\sqrt{t}$  and  $p$  are modified, keeping their ratio fixed], while the normalized steady-state, Eq. 9, is clearly time *invariant*. More importantly, the term infinite refers to the non-normalizability of the solution. Thus  $h(z)$ , while remaining positive, is certainly not a probability density. Its statistical meaning can be understood following the mathematical literature on infinite ergodic theory. In the long time, large momentum limit, with  $p/\sqrt{t}$  fixed,

$$\lim_{\substack{p, t \rightarrow \infty \\ p/\sqrt{t} \text{ fixed}}} t^{\tilde{U}_0/2} W(p, t) = h(p/\sqrt{t}) \quad (18)$$

The right-hand side is not normalized since the perfectly normalized PDF  $W(p, t)$  is multiplied by  $t^{\tilde{U}_0/2}$  which diverges as  $t \rightarrow \infty$ . The function  $h(z)$  is a density in the sense that it does provide some of the moments of the process  $p(t)$ , in particular those that diverge with respect to the integration over the steady-state. For example, the

second moment is

$$\langle p^2 \rangle = \begin{cases} \frac{1}{\tilde{U}_0 - 3} & \tilde{U}_0 > 3 \\ \frac{14\mathcal{N}}{2\tilde{U}_0\Gamma\left(\frac{\tilde{U}_0+1}{2}\right)} \frac{1}{2-\tilde{U}_0} (t/\tilde{U}_0)^{(3-\tilde{U}_0)/2} & 1 < \tilde{U}_0 < 3 \\ \frac{2(1-\tilde{U}_0)}{\tilde{U}_0} t & \tilde{U}_0 < 1. \end{cases} \quad (19)$$

For  $\tilde{U}_0 > 3$ , the kinetic energy is time-independent and is determined by the steady-state solution, and it blows up as  $\tilde{U}_0 \rightarrow 3$ . For the intermediate range,  $1 < \tilde{U}_0 < 3$ , the behavior is sub-diffusive, and the non-normalized state determines the kinetic energy. At the critical value  $\tilde{U}_0 = 1$  the system transitions to normal diffusive scaling of the mean-squared momentum.

Infinite densities are important in many applications beyond Sisyphus cooling, in particular in chaos theory (Akimoto, 2008; Korabel and Barkai, 2009). They have been studied extensively in the context of infinite ergodic theory (Aaronson, 1997), where the behavior of time averages is important. In the context of the system at hand, the steady-state solution and the infinite covariant density are complementary tools. Both are a long-time solution of the problem.  $W(p, t)$  converges towards the steady-state, as long as  $\tilde{U}_0 > 1$ . Similarly, plotted in the scaling form, the solution approaches the non-normalized infinite density (Fig. 5). For  $1 < \tilde{U}_0 < 3$ , the steady-state solution predicts an infinite energy but a finite normalization and the infinite density gives a finite energy but infinite normalization. Hence these two tools are complementary, and both are required for a complete description of the dynamics [Fig. 5 (bottom)].

Consider now the case of  $\tilde{U}_0 < 1$ . The steady-state (Eq. 11) is now not normalizable, an infinite invariant density describes the momentum distribution in the inner region  $p < \sqrt{t}$ , and there exists a limit

$$\lim_{t \rightarrow \infty} t^{(1-\tilde{U}_0)/2} W(p, t) \sim (1 + p^2)^{-\tilde{U}_0/2}. \quad (20)$$

The expression on the right hand side is a non-normalizable function since  $\tilde{U}_0 < 1$ , however it still describes a long-time limit of the density (Dechant et al., 2011a). It is not a coincidence that it is similar to the form found for the normalized steady-state (Eq. 11). Here infinite ergodic theory comes into play. In this branch of mathematics, there is a distinction between two types of observables: those that are integrable with respect to the non-normalized density and those that are not (the former is given on the right hand side of Eq. 20 and is time-independent). This is similar to the kinetic energy observable considered for the case  $\tilde{U}_0 > 1$  which, depending on the value of  $\tilde{U}_0$ , may be either integrable or non-integrable with respect to the infinite covariant density. The fluctuation behavior of the time-averages of observables was studied in (Aghion et al., 2019), a topic which goes beyond the scope of this Colloquium.

*Simulations and experiments.* As previously mentioned, the momentum power-law statistics were observed experimentally in (Douglas *et al.*, 2006) (Fig 4) and also simulated using quantum Monte Carlo simulations, in good agreement with Eq. 9. The authors concluded that the calculation presented a clear, statistically significant indication of the power-law tails of the momentum distribution. Simulations and calculations taking account of the underlying lattice structure of the laser field were performed in (Holz *et al.*, 2015). They performed Langevin simulations for shallow lattices showing agreement with the infinite covariant density of Eq. 16, proving that the lattice structure does not affect the scaling properties of the system. Experiments routinely observe the minimum point in the mean energy (*e.g.* the minimum in the inset of Fig. 2). In the shallow lattice regime, the predicted sudden sharp increase of the energy has been observed, using a single ion and tracking its position (Katori *et al.*, 1997). This has also allowed direct observation of a spatial Lévy-like trajectory (a 1d version of the dynamics of Fig 1), discussed in detail in Sec. III.B.

The non-Gaussianity of the momentum distribution of atoms in optical lattices was also studied in (Jersblad *et al.*, 2004) using  $^{133}\text{Cs}$ . They fit time-of-flight data to several test functions, including the power-law type distribution of Eq. 9 and a double Gaussian, concluding that a double Gaussian provides a better fit to the experimental data. Most of this investigation was performed far from the limit considered here of shallow lattices. The authors reported that, for  $U_0/E_R < 60$ , the atomic cloud does not reach a steady-state and atoms are eventually lost from the lattice by heating, possibly corresponding to the “divergence” point of the kinetic energy  $\tilde{U}_0 = 3$ . The double Gaussian picture is based on a correct physical insight relevant for the regime of deep lattices. There, the atoms are distributed between two modes: one with a population of trapped atoms (close to the minimum of the periodic field) and one of untrapped particles, giving rise to a pair of Gaussian momentum distributions. The regime  $\tilde{U}_0 < 1$  is predicted to exhibit special features, and experiments in this region are technically challenging. This is due to the fact that the system is actually being heated and atoms are easily lost from the trap. The issue of heating and loss of atoms is typically partially mediated by use of elongated dipole “tube” traps or blue-detuned optical box potentials (Afek *et al.*, 2020, 2017; Sagi *et al.*, 2012), however so far there is no clear-cut experimental proof of Eq. 20.

*Diffusion in a logarithmic potential.* The problem of momentum dynamics of Sisyphus-cooled ultracold atoms is related to the over-damped Langevin dynamics in a logarithmic potential (Bar *et al.*, 2007, 2008; Bray, 2000; Dechant *et al.*, 2011b; Fogedby and Metzler, 2007a,b; Hirschberg *et al.*, 2011, 2012; Poland and Scheraga,

1966). This connection stems from the fact that the friction force  $f(p) \sim -1/p$  at large  $p$ , and hence asymptotically the effective potential in momentum space is  $V(p) = -\int dp f(p) \sim \log(p)$ . More explicitly, consider a Brownian particle in a potential  $V(x) = V_0 \log(1+x^2)$  in contact with a standard thermal heat bath with temperature  $T$ . According to the Boltzmann-Gibbs framework, the density in thermal equilibrium is  $P_{\text{eq}} = \mathcal{N}(1+x^2)^{-V_0/k_B T}$ , bearing the same structure of the steady-state Eq. 9 with appropriate adjustments. The stochastic dynamics in a log potential is important for several problems, like DNA looping (Bar *et al.*, 2007; Hanke and Metzler, 2003) and Manning condensation (Manning, 1969).

## B. From Sisyphus friction to Lévy walks in position space

An immediate consequence of the anomalous dynamics in momentum space is nontrivial dynamics in real-space. In (Marksteiner *et al.*, 1996), the spatial diffusion of atoms was studied theoretically, revealing that below a critical depth of the optical lattice there exists a transition to a Lévy walk. To show this, certain modifications of the basic Lévy walk and, in particular, of Eq. 5 are needed. To have a clear physical picture, consider the experiment of (Sagi *et al.*, 2012) (Fig. 6), who studied the 1d diffusion of cold  $^{87}\text{Rb}$  atoms undergoing Sisyphus cooling. Starting with a narrow, thermally-equilibrated atomic cloud, the particles were released and their density profile imaged. In qualitative agreement with theory, a transition from normal to anomalous dynamics was observed and Lévy distributions were found to fit well to the experimental data.

In discussing the spatial dynamics, the Langevin description becomes crucial. Consider a long-time momentum-space trajectory  $p(t)$ , such that the momentum crosses zero many times. Let  $\tau$  be the random interval of time between two such successive crossings. Let  $-\infty < \chi < \infty$  be the random displacement for a given such interval, schematically presented in Fig. 7. We generate a process with a set of random jump durations  $\{\tau_i\}$  between zero crossings and corresponding displacements  $\{\chi_i\}$  given by  $\chi_1 = \int_0^{\tau_1} dp(t)$ ,  $\chi_2 = \int_{\tau_1}^{\tau_1+\tau_2} dp(t)$ , etc. For a particle starting at the origin at  $t = 0$  with  $p = 0$ , the sum of all the displacements  $\chi_i$  is the random position of the particle at time  $t = \sum_i \tau_i$ , denoted  $x(t)$ , and the corresponding PDF is  $P(x, t)$ . Since the Langevin process is driven by white noise, and is therefore infinitely unsmooth, defining zero crossings requires a more precise treatment (Barkai *et al.*, 2014; Kessler and Barkai, 2012; Majumdar and Comtet, 2004, 2005). We define the random time  $\tau$  as the time it takes the particle starting with momentum  $p = \epsilon$  to reach  $p = 0$  for the first time.

The Langevin process is Markovian, so once the particle crosses zero momentum, a given interval  $\tau$  is independent of the previous one. This is nothing but a renewal

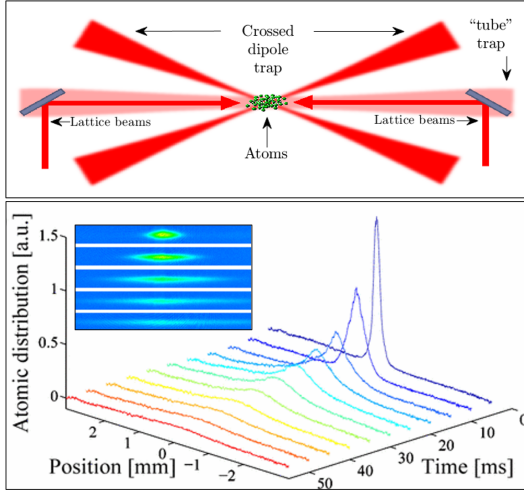


FIG. 6 Spatial dynamics. (Top) A sketch of the experimental setup used in (Afek *et al.*, 2020, 2017; Sagi *et al.*, 2012). Laser-cooled  $^{87}\text{Rb}$  atoms are loaded into a crossed optical dipole-trap and evaporatively cooled to thermal equilibrium. They are then transferred into a single-beam red-detuned and highly-elongated (“tube”) dipole-trap and propagate in a one-dimensional optical lattice with varying  $\tilde{U}_0$  for variable time. Their position distribution is then measured using fluorescence imaging (inset), and integrated to reveal the anomalous nature of the spreading (bottom)

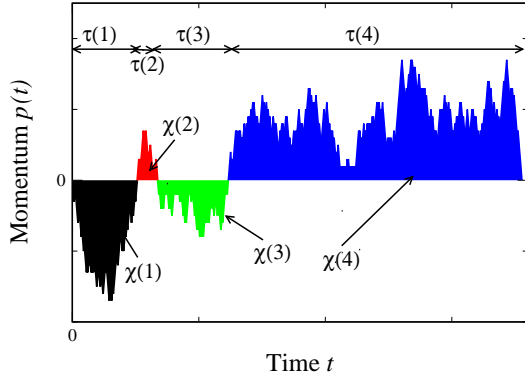


FIG. 7 Adapted from (Kessler and Barkai, 2012). Momentum zero-crossing dynamics reveal the nature of the spatial diffusion. The crossing of zero momentum defines durations  $\tau_i$  and jump lengths  $\chi_i$ , enabling identification of the connection between the continuous momentum path of the atom and the Lévy walk picture. Statistics of the crossing times can be obtained using first passage time theory. The PDF of the times  $\psi(\tau)$  is heavy tailed and the mean time diverges when  $\tilde{U}_0 < 1$ . The jump lengths are the areas under the stochastic momentum curve which starts and ends at zero momentum and never crosses in between. They are power-law distributed due to the weak friction at large momentum. The crossing times  $\{\tau\}$  and  $\{\chi\}$  are correlated, as the longer the crossing time the larger is the jump size, and  $\chi \sim \tau^{3/2}$ . This scaling differs from the standard Lévy walk which is ballistic  $\chi \sim \tau$ .

process:  $\tau_i$  is drawn repeatedly from  $\psi(\tau)$ , the crossing time PDF computed using the Langevin Eq. 10, until the sum of the times exceeds the measurement time. The distribution of crossing times can be calculated using the tools of first-passage theory (Martin *et al.*, 2011; Micciché, 2010; Redner, 2001). As shown by (Barkai *et al.*, 2014; Marksteiner *et al.*, 1996), the marginal PDFs of step durations and jump lengths exhibit power-law behaviors

$$\psi(\tau) \sim \tau^{-(3/2)-\tilde{U}_0/2}, \quad q(\chi) \sim |\chi|^{-(4/3)-\tilde{U}_0/3}. \quad (21)$$

This scaling is the result of the weak friction found at large momentum. In the limit  $\tilde{U}_0 = 0$ ,  $\psi(\tau) \sim \tau^{-3/2}$  which describes the distribution of first passage times of a Brownian particle in 1d searching for a target at the origin (Redner, 2001). This extremely shallow lattice limit describes a pure diffusive process in momentum space, with no friction. Long intervals are associated with large momenta, and so the cooling friction does not destroy the existence of power-law decay at large  $\tau$ , though it does change the actual exponent. The mean of  $\tau$  diverges when  $\tilde{U}_0 \leq 1$ , and the mean first passage time for the momentum, namely the time it takes the momentum to cross the origin, becomes infinite when the steady-state of the momentum distribution Eq. 11 is no longer normalized.

These scaling results immediately suggest a transition between a standard, Gaussian, random walk regime and a Lévy regime as  $\tilde{U}_0$  goes below 5. For  $\tilde{U}_0 > 5$ , the variance of  $\chi$  is finite, (since  $q(\chi) \sim |\chi|^{-3}$  when  $\tilde{U}_0 = 5$ ) and so, based on the central limit theorem argument presented in Sec. II.A, it is to be expected that a Gaussian position distribution of  $P(x, t)$  will be obtained in the long time limit. For  $\tilde{U}_0 < 5$ , on the other hand, the variance of  $\chi$  diverges, suggesting a Lévy flight scenario (at least as long as  $\tilde{U}_0 > 1$ , and the mean flight-duration  $\tau$  is finite).  $P(x, t)$  attains the self-similar scaling form (Kessler and Barkai, 2012):

$$P(x, t) \sim \frac{1}{(K_\nu t)^{1/\nu}} L_{\nu,0} \left[ \frac{x}{(K_\nu t)^{1/\nu}} \right]. \quad (22)$$

Here  $L_{\nu,0}(x)$  is the symmetric Lévy stable PDF of Eq. 4. The transport coefficient  $K_\nu$  describes the width of the packet, and is given in terms of the microscopic parameters of the model in (Kessler and Barkai, 2012). The Lévy exponent  $\nu = (\tilde{U}_0 + 1)/3$  is such that the solution approaches a Gaussian when  $\tilde{U}_0 \rightarrow 5$ .  $K_\nu$  vanishes as  $\tilde{U}_0 \rightarrow 1$  due to the divergence of the average  $\tau$ .

As discussed in Sec. II.A, power-law tails lead to infinite moments. The resolution of this paradox lies in the fact that the random variables  $\tau$  and  $\chi$  are in fact correlated, since longer flight durations lead to larger displacements. In fact, the largest jump in the process  $p(t)$  cannot be much larger than a length scale that in-

creases as  $t^{3/2}$  beyond which the tails of the Lévy PDF are naturally cut off as explained below. To see this, let us completely neglect the restoring friction force. Then the momentum undergoes pure diffusion, scaling like  $t^{1/2}$  and the jump size scales accordingly as  $t^{3/2}$ . This is a kind of Lévy walk, rather than a Lévy flight. It is different from the original Lévy walk discussed in Sec II.A, where the largest jump scales linearly with measurement time, since there the velocity is constant between turning points while here the motion is stochastic between any two zero crossings. This spatial regime, where the Lévy density (Eq. 22) holds, is therefore valid only up to a length scale that grows like  $t^{3/2}$ . This Lévy regime also shrinks as  $\tilde{U}_0$  increases, and vanishes as  $\tilde{U}_0 \rightarrow 5$ , beyond which only the Gaussian regime survives. To handle these correlations, one has to employ a powerful tool called the Montroll-Weiss equation (Hänggi and Marchesoni, 2005; Metzler and Klafter, 2000), relating the joint PDF of jump lengths and waiting times to the density of particles  $P(x, t)$  using the convolution theorem of Laplace and Fourier transforms. Going through the analysis of the Montroll-Weiss equation, one indeed finds that Eq. 22 is valid in the central regime (Fig. 8).

The analysis of the far tail of  $P(x, t)$  was carried out in (Aghion *et al.*, 2017), finding a spatial infinite (non-normalized) density. It showed a relation between the laser cooling process and the problem of the distribution of random areas under Langevin excursions (Agranov *et al.*, 2020; Barkai *et al.*, 2014; Majumdar and Comtet, 2005). The latter is a constrained Langevin process starting and ending at  $p = 0$ , never crossing the origin within a given time interval (Fig. 7). The derived cutoff of  $P(x, t)$  due to the above-mentioned correlations, ending the power-law Lévy regime, can be seen at the far right edge of the bottom panel of Fig. 8, and is in accord with direct simulations of the Langevin Eq. 10.

When  $\tilde{U}_0 < 1$ , correlations can never be neglected and then  $P(x, t) \sim (1/t^{3/2})g(x/t^{3/2})$  where  $g$  is some scaling function. In this limit of very shallow lattices,  $\tilde{U}_0 < 1$ , the momentum performs a random walk due to the random emission events, the friction is negligible, and then the momentum scales like  $\sqrt{t}$  as in Eq. 19. Hence, as shown analytically in (Barkai *et al.*, 2014), a cubic scaling of the MSD is obtained. This type of Richardson-like behavior was found by (Wickenbrock *et al.*, 2012) using Monte Carlo simulations, and the phase  $\tilde{U}_0 < 1$  is called the Richardson phase (Fig. 3). Richardson's law has thus far evaded measurement in atomic systems but has been experimentally observed in other contexts (Duplat *et al.*, 2013). The MSD therefore has three distinct phases: normal diffusion, superdiffusion and Richardson:

$$\langle x^2 \rangle \sim \begin{cases} t & 5 < \tilde{U}_0 \\ t^{(7-\tilde{U}_0)/2} & 1 < \tilde{U}_0 < 5 \\ t^3 & \tilde{U}_0 < 1. \end{cases} \quad (23)$$

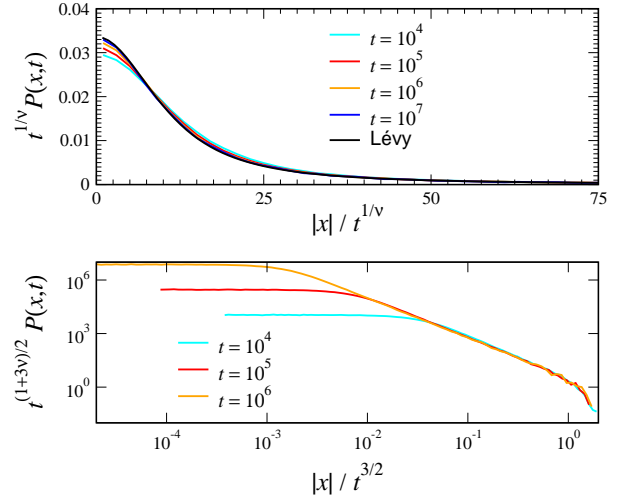


FIG. 8 Adapted from (Kessler and Barkai, 2012). Langevin simulations of the spatial dynamics. (Top) Results of numerical simulations of Eq. 10. Packets of particles starting from a common origin converge, in the long time limit, to a self-similar Lévy density presented as a solid line (Eq. 22,  $\nu = 7/6$ ). (Bottom) The simulated distribution exhibits also a second scaling, *i.e.* data collapse for several measurements times. Here the convergence is visibly faster for large  $x/t^{3/2}$  while for small values deviations from scaling are found. At large distances the power-law decay of the Lévy density is cut off due to finite time effects.

An intuitive argument for the behavior of the MSD in the regime  $1 < \tilde{U}_0 < 5$  can be obtained considering that the Lévy distribution of Eq. 22 describes the central part of the packet and that a cutoff exists at distances of order  $t^{3/2}$  (Fig. 8). From the power-law tail of the distribution, we can obtain  $P(x, t) \simeq tx^{-1-\nu}$  for  $x < t^{3/2}$ . Then  $\langle x^2 \rangle \simeq \int t^{3/2} dx x^2 P(x, t)$ , and using  $\nu = (\tilde{U}_0 + 1)/3$ , we find the result in Eq. 23. In short, the cutoff of the spatial Lévy distribution gives the correct time dependence of the MSD, but to calculate the MSD precisely, including prefactors, one needs to resort to the scaling Green-Kubo theory investigated in Sec IV.A.

The transition from normal to anomalous diffusion has been observed experimentally in (Katori *et al.*, 1997), where the motion of a single  $^{24}\text{Mg}^+$  ion was used to measure the scaling exponent of the MSD. It was observed to rise above unity below some threshold value of  $\tilde{U}_0$ , continuing to rise with decreasing  $\tilde{U}_0$ . The rise was roughly linear with  $\tilde{U}_0$ , and the slope consistent with the theoretical prediction of unity. Fig 9 depicts the exponent of the MSD of the trapped ion, as well as its time-traces showing a clear transition from normal statistics for deep lattices to rare-event dominated statistics for shallow ones.

The spatial dynamics was further explored in (Sagi *et al.*, 2012), confirming the transition between the normal Gaussian diffusion regime for deep enough lattices and the Lévy regime below some critical  $U_0$ . Both the



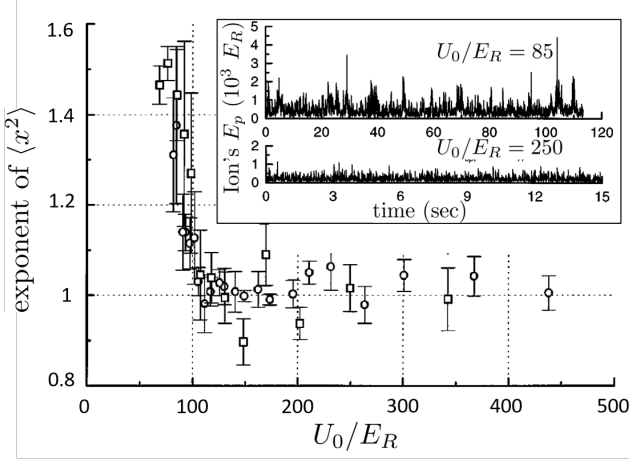


FIG. 9 Adapted from (Katori *et al.*, 1997). The exponent of  $\langle x^2 \rangle$  measured from the dynamics of a weakly harmonically trapped single  $^{24}\text{Mg}^+$  ion in a Sisyphus lattice. measurements are performed for short times such that the ion is effectively free and the trap is of marginal importance. For deep lattices, the dynamics is diffusive and  $\langle x^2 \rangle \sim t$ . As the lattice becomes shallower a steep rise in the exponent is observed as the dynamics become superdiffusive (Eq. 23). The inset shows the time traces of the potential energy of the ion as it moves in the trap. Large rare events are clearly visible in the shallow lattice (inset, top) corresponding to the heavy tails of the distributions, compared to the more Gaussian behavior of the deep lattice data (inset, bottom).

power-law scaling of the root-mean-squared displacement and the Lévy distribution of the displacement, with the Lévy index changing with lattice depth were observed, in agreement with theory. The scaling collapse and the resultant Lévy distributions are shown in the top panel of Fig. 10. The bottom panel shows the measured exponent of the time-dependent root-mean-squared displacement, as a function of  $U_0/E_R$ . The superdiffusive nature of the spatial spreading is also in agreement with the theoretical expectations, and, as well, the linear dependence of the exponent with  $U_0/E_R$  is in agreement with Eq. 23.

This agreement between theory and experiment, while encouraging, still remains incomplete. In particular, exponents above 2, and the saturation at a value of 3 associated with the Richardson phase, have yet to be observed. This is not totally unexpected, since if the particles are moving super-ballistically, they will quickly leave the trap, and may go undetected (Sagi *et al.*, 2012). A possible way to alleviate this may arise in the form of optically-engineered potentials which create strong confinement as well as reflecting boundary-conditions for the atomic packet (Gaunt *et al.*, 2013; Livneh *et al.*, 2018).

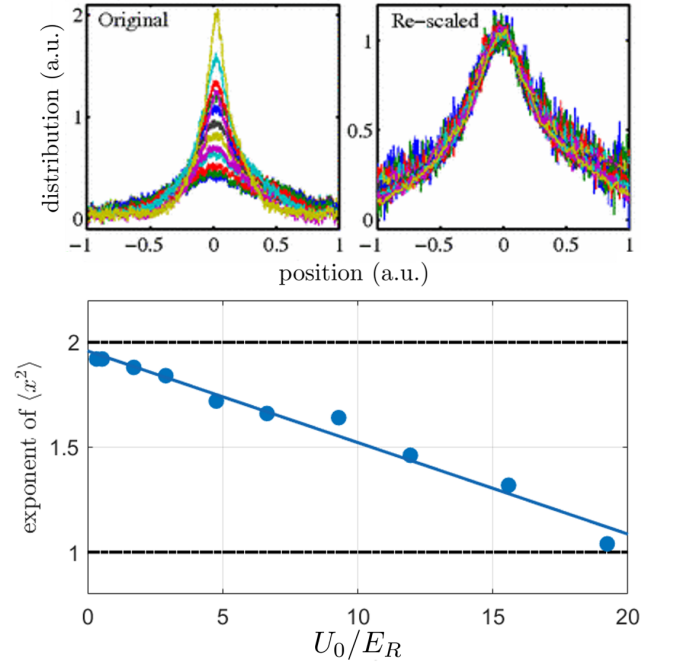


FIG. 10 Adapted from (Sagi *et al.*, 2012). Self-similarity, Lévy distributions and superdiffusion. The temporal scaling of  $\langle x^2 \rangle$  is measured in 1d using the setup shown in Fig. 6. (top) Data collapse of the spatial distributions as a function of time for the rescaling transformation  $x \rightarrow x/t^{1/\nu}$  (Eq. 22 and Fig. 8), with  $\nu = 1.25$  in a  $U_0/E_R = 4.8$  lattice. (bottom) The extracted exponent of  $\langle x^2 \rangle$ .  $C$  is used as a fitting parameter for Eq. 23, giving a value of  $11 \pm 1$  for this measurement. The experiment also observed the power-law tails of the spatial distribution predicted by Eq. 22

### C. Position-momentum correlations

As both the momentum (Eq. 19) and position (Eq. 23) dynamics are governed by power-laws, the cross-correlation  $C_{xp}$  between position and momentum should also behave in a similar way. Defined according to

$$C_{xp}(t) \equiv \frac{\langle x(t)p(t) \rangle}{\sqrt{\langle x^2(t) \rangle \langle p^2(t) \rangle}}, \quad (24)$$

this Pearson correlation asymptotically decays as  $1/\sqrt{t}$  for normal diffusion (Gillespie and Seitaridou, 2012) and approaches unity for ballistic and Richardson-type motion. This observable is in general challenging to access experimentally as it requires knowledge of the position of a group of atoms contained in a certain narrow momentum bin.

In (Afek *et al.*, 2017), a scaling relation was derived describing the asymptotic dynamics of  $C_{xp}(t \rightarrow \infty)$  for the general case where both position and momentum have power-law long-time behavior:  $\langle x^2(t) \rangle \sim t^{2\alpha_x}$  and  $\langle p^2(t) \rangle \sim t^{2\alpha_p}$ . Here the exponents  $\alpha_i$  describe anomalous processes in general. Substituting those into Eq. 24, along with the fact that  $\langle xp \rangle \sim d\langle x^2 \rangle/dt \sim t^{(2\alpha_x-1)}$ , gives

$C_{xp} \sim t^{\alpha_x - \alpha_p - 1}$ . In terms of  $\tilde{U}_0$ , it should then scale like

$$C_{xp}(t) \sim \begin{cases} \text{const} & \tilde{U}_0 < 3 \\ t^{(3-\tilde{U}_0)/4} & 3 < \tilde{U}_0 < 5 \\ t^{-1/2} & \tilde{U}_0 > 5. \end{cases} \quad (25)$$

As  $\tilde{U}_0$  is varied, the behavior ranges from “normal”, a  $t^{-1/2}$  decay, to a constant. This has been numerically verified in a new analysis of the simulations performed in (Afek *et al.*, 2017) and is shown in the bottom panel of Fig. 11.

The correlation function is however not merely a tool to explore the long-time dynamics. Rather, it yields information about the short-time behavior as well. An additional feature discussed in (Afek *et al.*, 2017) relates to the short-time dynamics of a system of particles released from a harmonic trap and allowed to propagate in the Sisyphus lattice. At times short compared to the oscillation period in the trap before release, ( $t < 1/\omega$ ), correlations build up linearly regardless of the depth of the lattice as the diffusive dynamics are as yet unfelt by the atoms ( $\omega$  sets, in accordance with the equipartition theorem, the ratio between the initial standard-deviation of the momentum distribution and that of the position distribution). At longer times, diffusion kicks in and the behavior of Eq. 25 is expected to take over.

Fig. 11 (top panel) shows the measured position-momentum correlations as an atomic cloud evolves in lattices of different  $\tilde{U}_0$ . The initial buildup of correlations is evident for all lattice depths considered, as well as its following decay. The  $\tilde{U}_0 = 0$  data set is expected (and shown) to be ballistic. The position-momentum phase space distributions on the right are measured using a tomographic reconstruction of the phase-space density distribution function of the atomic ensemble (Afek *et al.*, 2017). The upper phase space distribution reveals a high correlation corresponding to ballistic expansion while the lower one shows the destruction of the correlation by the diffusive dynamics.

#### IV. IMPLICATIONS FOR FUNDAMENTAL CONCEPTS IN STATISTICAL PHYSICS

##### A. Scaling Green-Kubo relation

As mentioned in Sec. I, the Green-Kubo relation, which first appeared in (Taylor, 1922) in the context of diffusion in a turbulent medium, relates the diffusion constant of a particle,  $D = \langle x^2(t) \rangle / 2t$ , to an integral over the stationary time correlation function of the velocity (or, equivalently in our case, momentum)  $C_p(t, t + \tau) =$

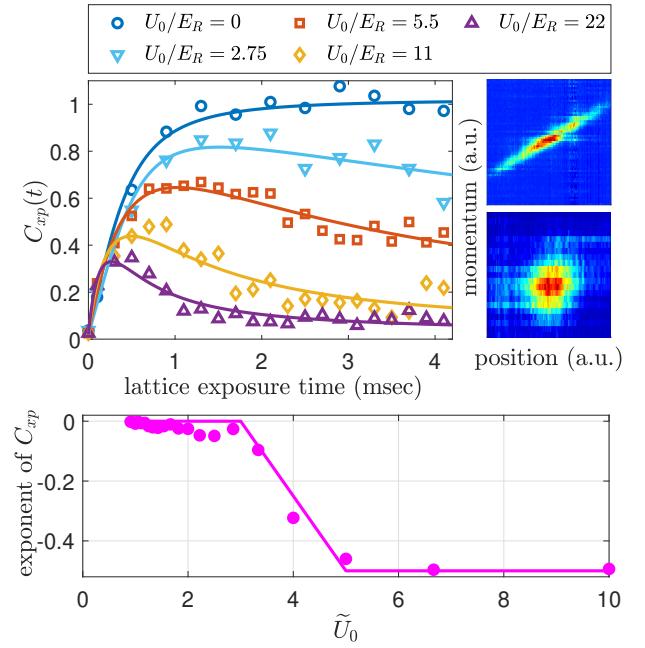


FIG. 11 Adapted from (Afek *et al.*, 2017). Position-momentum correlations. (Top) Experimental results for the position-momentum correlations as a function of lattice exposure time and lattice depth  $U_0/E_R$ . At short times the correlations build up and are later quenched at varying rates, depending on the anomalous dynamics. The images on the right are the tomographically-measured phase space probability densities for ballistic expansion (upper) and  $U_0/E_R = 5.5$  (lower), at a lattice exposure time of 4.1 msec, showing the effect of the lattice on the development of the correlations. (Bottom) Langevin simulation (circles) validating the prediction of Eq. 25 depicted by the solid line.

$$\langle p(t)p(t + \tau) \rangle \quad (\text{Green, 1954; Kubo, 1957}),$$

$$D = \frac{1}{M^2} \int_0^\infty d\tau C_p(t, t + \tau) \quad (26)$$

In the case of a Brownian particle of mass  $M$  with Stokes' friction coefficient  $\gamma_s$ , the momentum correlation function is exponential,  $C_p(t, t + \tau) = k_B T M e^{-\gamma_s \tau}$ , and the Green-Kubo formula gives the Einstein relation  $D = k_B T / (M \gamma_s)$  linking the diffusivity and the friction coefficient via the temperature  $T$ . For  $\tilde{U}_0 > 3$ , this standard Green-Kubo relation applies. For  $\tilde{U}_0 < 3$ , however, it breaks down, owing to one of two reasons: either because the correlation function is not stationary, or alternatively, while the correlation function is stationary, its time-integral diverges. Depending on the value of  $\tilde{U}_0$ , either scenario can occur, and in both cases Eq. 26 needs to be generalized (Dechant *et al.*, 2014).

Consider the general momentum correlation function

$$C_p(t_2, t_1) = \int_{-\infty}^{\infty} dp_2 dp_1 p_2 p_1 P(p_2, t_2 | p_1, t_1) P(p_1, t_1 | 0, 0) \quad (27)$$

where  $P(p_2, t_2 | p_1, t_1)$  is the probability of the particle having momentum  $p_2$  at time  $t_2$ , given that it had momentum  $p_1$  at time  $t_1$ . The notation  $P(p_2, t_2 | p_1, t_1)$  is used here, as opposed to the  $W(p, t)$  used earlier, to explicitly indicate the dependence on the initial momentum and time.  $\langle x^2(t) \rangle$  can then be calculated from  $C_p(t_2, t_1)$ . In the case where the process is stationary at long times, so that the stationary momentum distribution (denoted by the subscript  $s$ ) exists and is given by  $\lim_{t_1 \rightarrow \infty} P(p_1, t_1 | 0, 0) = W_s(p_1)$ , then  $C_p(t_2, t_1) = C_{p,s}(|t_2 - t_1|)$  only depends on the time lag  $\tau = t_2 - t_1$

$$C_{p,s}(\tau) = \int_{-\infty}^{\infty} dp_2 \int_{-\infty}^{\infty} dp_1 p_2 p_1 P(p_2, \tau | p_1, 0) W_s(p_1) \quad (28)$$

Since  $x(t)$  is the time-integral of  $p(t)/M$ ,

$$\langle x^2(t) \rangle = \frac{1}{M^2} \int_0^t dt_2 dt_1 C_{p,s}(|t_2 - t_1|) = \frac{2t}{M^2} \int_0^t d\tau C_{p,s}(\tau) \quad (29)$$

from which follows the standard Green-Kubo formula, Eq. 26.

What then is the form of the momentum correlator  $C_p(t_2, t_1)$  in the Sisyphus system? Turning to the definition of Eq. 27, we have already seen how to calculate from the Fokker-Planck Eq. 8 the factor  $W(p_1, t_1)$ . For large  $p_1$ , this decays as a power-law with a Gaussian fall-off at  $p_1 \sim O(\sqrt{t_1})$  (Eqs. 14, 16 and 17). The calculation of the other factor  $P(p_2, p_1; t_2 - t_1)$  is similar, and it behaves similarly for large  $p_2$  as long as  $p_1$  is not too large, which is the relevant regime since the  $P(p_1, t_1 | 0, 0)$  factor in Eq. 27 cuts it off. The detailed calculation (Dechant *et al.*, 2011b, 2012) reveals that the correlator has the following form:

$$C_p(t_2, t_1) \approx \begin{cases} C_{\alpha>1} t_1^{2-\alpha} g_{\alpha>1} \left( \frac{t_2 - t_1}{t_1} \right), & \alpha > 1 \\ C_{\alpha<1} t_1 g_{\alpha<1} \left( \frac{t_2 - t_1}{t_1} \right), & \alpha < 1 \end{cases} \quad (30)$$

where  $\alpha \equiv \frac{\tilde{U}_0 + 1}{2}$ , and

$$\begin{aligned} C_{\alpha>1} &= \frac{\mathcal{N}(4D_0/p_c)^{2-\alpha} \sqrt{\pi}}{\Gamma(\alpha+1)\Gamma(\alpha)/p_c} \\ C_{\alpha<1} &= \frac{4D_0 \sqrt{\pi}}{\Gamma(\alpha+1)\Gamma(1-\alpha)} \\ g_{\alpha>1}(s) &= s^{2-\alpha} \int_0^\infty dy y^2 e^{-y^2} {}_1F_1 \left( \frac{3}{2}; \alpha+1; y^2 \right) \Gamma(\alpha, y^2 s) \\ g_{\alpha<1}(s) &= s \int_0^\infty dy y^2 e^{-y^2} {}_1F_1 \left( \frac{3}{2}; \alpha+1; y^2 \right) e^{-y^2 s}. \end{aligned} \quad (31)$$

${}_1F_1$  is the confluent hypergeometric function, and  $\mathcal{N}$  is the normalization factor given below Eq. 11. The correlation function is, in general, non-stationary. The dependence of the correlator on the relative time  $s = (t_2 - t_1)/t_1$  is called “aging” (Bouchaud, 1992). Normally the aging correlator has the form  $\langle C_p(t_2, t_1) \rangle \sim \langle p^2 \rangle_{eq} g(s)$  (Bouchaud, 1992; Burov *et al.*, 2010; Margolin and Barkai, 2004), however here it takes the form

$$C_p(t_2, t_1) \sim t_1^\phi g(s) \sim \langle p^2(t_1) \rangle g(s), \quad (32)$$

with  $\phi = \min(2 - \alpha, 1)$ , and  $g(s)$  is either  $g_{\alpha>1}$  or  $g_{\alpha<1}$  depending on whether  $\alpha$  is greater or smaller than unity. To mark this added dependence on  $t_1$ , due to the growth of  $\langle p^2(t_1) \rangle$  with time, this phenomenon is termed “super-aging”.

Let us consider the limit  $t_2 - t_1 \ll t_1$ ,

$$C_p(t_2, t_1) \approx \begin{cases} \frac{\pi \Gamma(\alpha-2)}{4 \mathcal{N} \Gamma^2(\alpha-\frac{1}{2})} [4D_0(t_2 - t_1)]^{2-\alpha} & \alpha > 2 \\ \frac{1}{\mathcal{N} \Gamma(\alpha) \Gamma(2-\alpha)} (4D_0 t_1)^{2-\alpha} & 1 < \alpha < 2 \\ (1-\alpha)(4D_0 t_1) & \alpha < 1 \end{cases} \quad (33)$$

For  $\alpha > 2$ , the correlation function is stationary in this limit, a fact that will be important for the discussion of ergodicity breaking in Sec. IV.B. For  $\alpha < 2$ , on the other hand, even the limiting correlation function is nonstationary and dominated by the growth in time of  $\langle p^2(t_1) \rangle$ , leading to super-aging.

The super-aging of the correlation function (Eq. 32) has some interesting consequences on the MSD (Dechant *et al.*, 2014). For  $t \gg 1$ ,

$$\begin{aligned} \langle x^2(t) \rangle &\simeq \frac{2C_f}{M^2} \int_0^t dt_2 \int_0^{t_2} dt_1 t_1^\phi g \left( \frac{t_2 - t_1}{t_1} \right) \\ &\simeq \frac{2C_f}{M^2} \int_0^t dt_2 t_2^{\phi+1} \int_0^\infty ds (s+1)^{-\phi-2} g(s) \\ &\simeq 2D_\phi t^{\phi+2} \end{aligned} \quad (34)$$

with

$$D_\phi \equiv \frac{\mathcal{C}_f}{M^2(\phi+2)} \int_0^\infty ds (s+1)^{-\phi-2} g(s). \quad (35)$$

Here,  $\mathcal{C}_f$  is either  $\mathcal{C}_{\alpha>1}$  or  $\mathcal{C}_{\alpha<1}$ , as appropriate. This reproduces the scaling behavior of Eq. 23 on general grounds from the Lévy scaling and the cutoff, adding to it the calculation of  $D_\phi$ .

Eq. 34 is the scaling form of the Green-Kubo relation. It is applicable for  $\phi > -1$ , which corresponds to superdiffusion. The usual diffusion coefficient in Eq. 26 is then ill-defined, and is replaced by the anomalous diffusion coefficient  $D_\phi$ . In resemblance with the original Green-Kubo formula,  $D_\phi$  is given in terms of an integral over a function of a single variable. Determining the diffusive behavior of a system from its correlation function thus amounts to determining the exponent  $\phi$  and the scaling function  $g(s)$ . While Eq. 34 was derived in terms of momentum and position, it holds for any two quantities where one is up to a constant factor the time integral of the other. An example of such analogy, between frequency and phase, is given in Sec. V.A. The different scaling regimes for the MSD for the Sisyphus problem are thus seen to be related to the properties of the correlator. For  $\alpha > 3$  ( $\tilde{U}_0 > 5$ ), the correlator is stationary, the integral in the standard Green-Kubo formula converges and the diffusion is normal. The spatial diffusion constant diverges as  $\alpha \rightarrow 3$  from above, due to the factor  $s^{2-\alpha}$  in  $g$ , signalling the breakdown of normal diffusion. For  $1 < \alpha < 3$  ( $1 < \tilde{U}_0 < 5$ ), the standard Green-Kubo formula breaks down and the exponent  $\phi = 2 - \alpha$ . The MSD then scales as  $t^{4-\alpha}$ , and the dynamics are superdiffusive, with an anomalous diffusion constant given by (plugging in the value of  $\mathcal{N}$ )

$$D_\phi = \frac{(4D_0)^{2-\alpha} p_c^{2\alpha-2} \Gamma(\alpha-1/2)(\alpha-1)}{\Gamma^3(\alpha)\alpha(4-\alpha)M^2} \int_0^\infty ds (s+1)^{\alpha-4} g_{\alpha>1}(s). \quad (36)$$

This anomalous diffusion constant vanishes at  $\alpha = 1$  ( $\tilde{U}_0 = 1$ ) and, due to the factor  $s^{2-\alpha}$  in  $g_{\alpha>1}(s)$ , diverges as  $\alpha \rightarrow 3$ .

For  $\alpha < 1$  ( $\tilde{U}_0 < 1$ ), the anomalous diffusion exponent saturates at a value of 3, corresponding to Richardson diffusion. The anomalous diffusion constant in this regime is

$$D_\phi = \frac{4D_0\sqrt{\pi}}{3\Gamma(\alpha)\Gamma(1-\alpha)M^2} \int_0^\infty ds (s+1)^{-3} g_{\alpha<1}(s). \quad (37)$$

Using techniques such as Raman velocity selection (Kasevich *et al.*, 1991), cold atom experiments have the potential for directly observing the momentum correlation function and through it the Green-Kubo relation,

as it is based on the ability to perform selective state transitions of specifically targeted velocity classes of atoms.

## B. Breakdown of ergodicity

Systems in equilibrium visit all of phase space, with the average relative frequency of visiting any certain point given by the Boltzmann-Gibbs distribution. Thus, over long enough observation times, the time-averages of observables correspond to the equilibrium ensemble averages. In systems with anomalous diffusion, however, this is no longer necessarily the case (Metzler *et al.*, 2014). The time-average, even in the infinite time limit, varies from realization to realization. This was studied in the context of sub-recoil laser cooling (Saubamea *et al.*, 1999), fluorescence intermittency in quantum dots (Brokmann *et al.*, 2003) and in single-atom motion in non-dissipative optical lattices (Kindermann *et al.*, 2016). Ergodicity breaking in Sisyphus cooling was first theoretically investigated in (Lutz, 2004). An alternative analysis taking into account the essential time-dependence of the momentum distribution at large momenta is given in (Dechant *et al.*, 2011b, 2012).

To probe the possibility of ergodicity breaking for the momentum, consider the ensemble variance of  $\bar{p} - \langle p \rangle$  for a particle that starts with momentum  $p = 0$  at  $t = 0$ , where the bar refers to the time average and the angle brackets to the ensemble average. Ergodicity is broken when this quantity, which due to reflection symmetry reduces to

$$\langle \bar{p}^2 \rangle = \lim_{T \rightarrow \infty} \frac{1}{T^2} \langle x^2 \rangle, \quad (38)$$

deviates from zero. Given Eq. 23 describing the spatial MSD, we find (Dechant *et al.*, 2012)

$$\langle \bar{p}^2 \rangle \sim \begin{cases} t^{-1} & \alpha > 3 \\ t^{2-\alpha} & 1 < \alpha < 3 \\ t & \alpha < 1 \end{cases} \quad (39)$$

with  $c_\alpha$  an  $\alpha$ -dependent constant. The  $1/t$  behavior seen for  $\alpha > 3$  ( $\tilde{U}_0 > 5$ ) is the “normal” behavior. For  $2 < \alpha < 3$ , ergodicity is achieved, albeit anomalously slower. For  $\alpha < 2$ ,  $\langle \bar{p}^2 \rangle$  does not vanish as  $t \rightarrow \infty$  and ergodicity is broken.

## C. Violation of the equipartition theorem

Up to this point we have discussed free, untrapped systems (with the exception of the trapped ion system of Fig. 9). It is natural to now address the question of to what extent this behavior is modified in the presence of an external binding potential. This question has been studied theoretically in its simplest context, that of a har-



monic well, in (Dechant *et al.*, 2015, 2016). This work focuses on the steady-state phase-space distribution of the particles, and in particular the breakdown of equipartition. The dynamics and violation of the equipartition of the system's energy have also been probed experimentally in (Afek *et al.*, 2020).

The experimental parameters are  $\mathcal{A}$ , the strength of the linear friction,  $p_c$ , the momentum scale for the onset of the nonlinear friction (Eq. 6),  $\omega$ , the harmonic oscillation frequency of the atoms in the trap, and  $D_0$  that controls the noise. Consider the scaled coordinates  $x \rightarrow m\omega x/p_c$  and  $p \rightarrow p/p_c$ . There are now two dimensionless parameters which characterize the dynamics, the familiar  $\tilde{U}_0$  and a new parameter controlling the strength of the harmonic trap,  $\Omega = \omega/\mathcal{A}$ . The Fokker-Planck equation is modified to a Kramers-Fokker-Planck (KFP) equation for the phase-space density, which in these scaled coordinates reads:

$$\frac{\partial}{\partial t} P(x, p, t) = \left[ \Omega \left( -p \frac{\partial}{\partial x} + x \frac{\partial}{\partial p} \right) + \frac{\partial}{\partial p} \left( \frac{p}{1+p^2} + \frac{1}{\tilde{U}_0} \frac{\partial}{\partial p} \right) \right] P(x, p, t). \quad (40)$$

The theoretical analysis focuses on the properties of the steady-state solution, that breaks down for shallow lattices, where a steady-state momentum distribution does not exist. An analysis of the time-dependent problem, which is required to treat  $\tilde{U}_0 < 1$ , has not yet been performed.

As the steady-state of the KFP equation is not exactly solvable, the analysis is restricted to various limits, the first of which is the low noise limit,  $\tilde{U}_0 \gg 1$ , where  $x$  and  $p$  are both of the order  $1/\sqrt{\tilde{U}_0}$ . Defining  $\hat{x} = x\sqrt{\tilde{U}_0}$  and  $\hat{p} = p\sqrt{\tilde{U}_0}$ , to first order in  $1/\tilde{U}_0$  (Dechant *et al.*, 2015, 2016)

$$P(\hat{x}, \hat{p}) \simeq e^{-\frac{\hat{x}^2 + \hat{p}^2}{2}} \left\{ 1 + \frac{1}{4(3+4\Omega^2)\tilde{U}_0} [3\hat{p}^4 + 18\hat{x}^2 - 27 + \Omega(4\hat{p}^3\hat{x} - 12\hat{p}\hat{z}) + 3\Omega^2((\hat{x}^2 + \hat{p}^2)^2 - 8)] \right\} \quad (41)$$

In contrast to the zeroth order term, which is a function of the Hamiltonian  $\mathcal{H} = (\hat{x}^2 + \hat{p}^2)/2$ , the correction term is not. Only in the limit of large  $\Omega$  does the correction term become a function of  $\mathcal{H}$  alone. The fact that the density is not only a function of  $\mathcal{H}$  implies that energy equipartition is not necessarily preserved. Defining the *equipartition parameter* as the square-root of the ratio of the expectation value of the kinetic energy,  $E_k$ , over that of the potential energy,  $E_p$  in a harmonic potential,

$$\chi_H = \sqrt{E_k/E_p} = \sqrt{\langle p^2 \rangle / \langle x^2 \rangle} \quad (42)$$

we find that, up to second order in  $1/\tilde{U}_0$

$$\chi_H \simeq 1 - \frac{3}{3+4\Omega^2} \tilde{U}_0^{-2} \quad (43)$$

Thus, the first-order term above does not induce a breakdown of equipartition, but the higher-order terms do.

Another limit is the large  $\Omega$  limit for arbitrary  $\tilde{U}_0$ , (whereas above, we looked at the large  $\Omega$  limit for  $\tilde{U}_0 \gg 1$ ) corresponding to weak damping. To leading order,  $P(x, p)$  is function of  $\mathcal{H}$  only,

$$P(x, p) \simeq \frac{1}{2\pi Z} \left( 1 + \sqrt{1 + x^2 + p^2} \right)^{-2\tilde{U}_0} \quad (44)$$

where the partition function  $Z = 2^{-2\tilde{U}_0} \tilde{U}_0 / (\tilde{U}_0 - 1)(2\tilde{U}_0 - 1)$ . This partition function diverges for  $\tilde{U}_0 \leq 1$ , above which (as in the unconfined case) the steady-state solution is non-normalizable and the dynamics are intrinsically time-dependent. The marginal momentum distribution decays as  $|p|^{-2\tilde{U}_0+1}$ , markedly different from the  $|p|^{-\tilde{U}_0}$  asymptotics without the confining potential. In particular, the steady-state average kinetic energy diverges for  $\tilde{U}_0 < 2$  for the confined system whereas it diverges already for  $\tilde{U}_0 < 3$  for the unconfined case. The same power-law behavior holds for the marginal distribution of  $x$  in this underdamped limit, given that  $P(x, p)$  is a function of  $x^2 + p^2$  only. This asymptotic power-law behavior for  $x$  and  $p$  holds, in fact, even beyond the large- $\Omega$  limit, because at high energies the damping is typically small. The high-energy regime is therefore an underdamped regime as well, and the results for  $\Omega \gg 1$  can be shown to hold (Dechant *et al.*, 2015).

Experimentally, observing such a violation of equipartition requires the ability to measure  $\langle x^2 \rangle$ ,  $\langle p^2 \rangle$  and  $\omega$ . The experimental situation described in (Afek *et al.*, 2020) is actually more complicated, as the optical dipole potential applied there is anharmonic, and so the conveniently measurable quantity of Eq. 42 is only an approximation. In the experiment,  $^{87}\text{Rb}$  atoms are evaporatively cooled in a far detuned, 1064 nm crossed dipole trap overlapped with a strong, loosely focused “tube trap”. The long evaporation time leaves the atoms in thermal equilibrium with the confining potential. They are then coupled to a 1d dissipative Sisyphus lattice. The measured steady-state values of  $\chi_H$  are shown in Fig. 12. In accord with the theory,  $\chi_H$  is found to be less than its thermal value, and the breakdown of equipartition becomes stronger with increasing lattice depth. Experimentally it is even easier to probe the dynamics of the equipartition than the steady-state (Afek *et al.*, 2020), leaving room for theory to catch up.

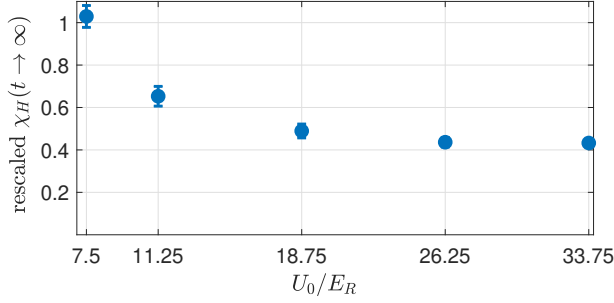


FIG. 12 Adapted from (Afek *et al.*, 2020). Steady-state values of the equipartition parameter  $\chi_H$  measured for a trapped cloud of  $^{87}\text{Rb}$  atoms, rescaled by its thermal value (less than unity due to trap anharmonicity), quantifying deviation from equipartition. Deep lattices significantly decrease the value of  $\chi_H$  compared to the thermal value. For even deeper lattices, inaccessible in the experiment,  $\chi_H$  is predicted to approach unity as well.

## V. LÉVY STATISTICS AND POWER-LAWS IN OTHER ATOMIC SYSTEMS

### A. Motional broadening in two-level system ensembles with a heavy-tailed frequency distribution

Consider an oscillator whose frequency has some anomalous stochastic dynamics. This frequency, together with the phase of the oscillator which is its time integral, are analogous to the momentum and position whose dynamics were discussed above. The phase spreads, similarly to the spatial spread of the particle packet, leading to decoherence, which is a limiting factor in many applications such as atomic clocks and quantum memories based on two-level systems (Heshami *et al.*, 2016; Ludlow *et al.*, 2015). In the typical case, when the homogeneous frequency distribution of the ensemble has finite moments, stochastic fluctuations cause the phase spread to grow diffusively  $\Delta\phi \sim t^{1/2}$  as compared to ballistic spread  $\Delta\phi \sim t$  for static frequency inhomogeneity (Sagi *et al.*, 2010). This slower diffusive spread induces the well known effect of *motional narrowing* of the power spectrum that also lengthens ensemble coherence times (Bloembergen *et al.*, 1948; Romer and Dicke, 1955). When the homogeneous frequency distribution of the ensemble is heavy-tailed, however, the picture is different. The stochastic phase dynamics becomes anomalous, the phase spread grows super-diffusively, and motional narrowing is hindered (Sagi *et al.*, 2011). In particular, when the first moment of the frequency distribution diverges, the stochastic frequency fluctuations can lead to broadening of the spectrum (*motional broadening*), surprisingly shortening the coherence time as the rate of fluctuations increases (Burnstein, 1981; Sagi *et al.*, 2011). For a frequency distribution following Lévy statis-

tics  $\exp(-A|\kappa|^\nu)$  as in Eq. 3, the transition between motional narrowing and motional broadening occurs at  $\nu = 1$ , corresponding to the Lorentzian spectrum. The coherence time of the ensemble decays as  $\tau_c^{\nu-1}$  (Sagi *et al.*, 2011) with  $\tau_c$  being the correlation time of the fluctuating frequency.

This slowing down or accelerating of the ensemble coherence decay depending on the value of  $\nu$  is a particularly striking feature. In this respect, the fluctuations act as resetting events such that motional narrowing is analogous to the Zeno effect (Milburn, 1988) in which certain events, such as measurements, delay the decay of a system. By the same token, motional broadening is analogous to the anti-Zeno effect (Sagi *et al.*, 2011), where the opposite occurs.

It has been theorized (Poletti *et al.*, 2013, 2012) and recently verified experimentally (Bouganne *et al.*, 2020) with ultracold atoms in optical lattices that strong interactions in a many-body system can also generate an anomalous decay of the coherence of the ensemble. Long-range interactions in ion chains have recently been used to probe the assumption that classical hydrodynamics can emerge universally for any complex quantum system, due to mixing of local degrees of freedom through the cleverly-engineered power-law decaying Ising interactions (Joshi *et al.*, 2021). Power-law spectral line shapes can naturally emerge in NMR due to dipolar interactions (Klauder and Anderson, 1962), long range interactions (Holtmark, 1919) and various other homogeneous imperfections (Stoneham, 1969). They are also related to ergodicity breaking in blinking quantum dots (Margolin and Barkai, 2005) and to the dynamics of photons in warm atomic vapor (Baudouin *et al.*, 2014; Mercadier *et al.*, 2009).

### B. Lévy dynamics in sub-recoil laser cooling

Sub-recoil laser cooling (Aspect *et al.*, 1988; Kasevich and Chu, 1992) relies on a totally different mechanism than that of the sub-Doppler cooling, and still it is rewarding that some of the general insights gained here can be applied there, showing the generality of our toolbox. In particular, Lévy laws are known to govern the statistical aspects of the problem, an issue previously analyzed extensively by Cohen-Tannoudji and collaborators (Bardou *et al.*, 2002). However, the rule of infinite ergodic theory and the underlying non-normalized state was only very recently connected to this system (Barkai *et al.*, 2021). The new analysis shows that in sub-recoil laser cooling there exists a non-normalised state describing some of the coldest atoms, that is complementary to the standard description of the problem (Bardou *et al.*, 1994).

Sub-recoil laser cooling is based on carefully engineering the photon scattering rate of an atomic ensemble in

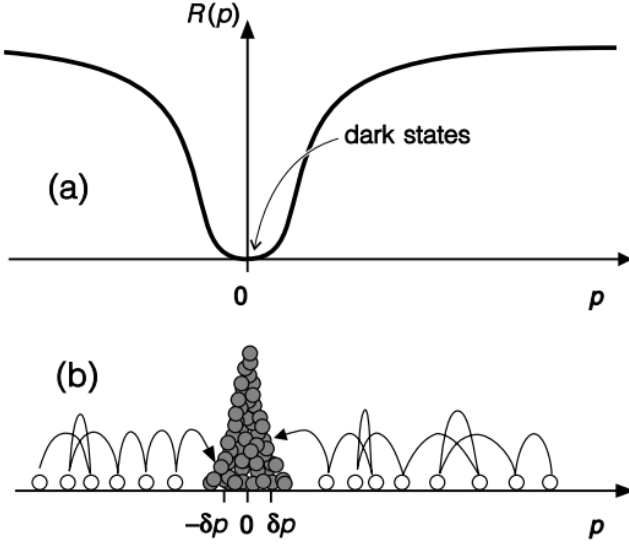


FIG. 13 Adapted from (Bardou *et al.*, 2002). Sub-recoil laser cooling. (a) The fluorescence rate  $R(p)$  vanishes for  $p = 0$ . (b) The atoms perform a random walk in momentum-space and accumulate in a small interval around  $p = 0$  where they remain trapped

such a way that slow (cold) atoms have a smaller chance of absorbing a photon from the laser than hot ones. In other words, the photon scattering rate  $R(p) \xrightarrow{p \rightarrow 0} 0$ . An atom will diffuse due to random kicks from photon recoil events until its momentum becomes small enough that the scattering rate diminishes significantly, and it will linger for a lengthy period of time at low momentum and remain cold (Fig. 13). The characteristic evolution time of an atom in such a laser field is  $R^{-1}(p)$ , which diverges as  $p$  approaches zero. Depending on the small- $p$  behavior of the scattering rate, the distribution of these waiting times may have heavy tails and even diverging moments, a signature of anomalous, Lévy-type dynamics.

More specifically, the rate  $R(p) \sim |p|^\zeta$  and  $\zeta$  can be controlled experimentally (Bardou *et al.*, 1994; Cohen-Tannoudji and Guéry-Odelin, 2011; Reichel *et al.*, 1995). Here, one finds a non-normalized state which is controlled by the value of  $\zeta$ . In particular, sub-recoil laser cooling works best when the mean time in the momentum trap diverges. This means on the one hand long stagnation times during which the speeds are close to zero, which is of course the goal of cooling, but at the same time indicates the violation of the basic postulates of statistical physics.

The theoretical challenge is therefore to construct a statistical theory to replace ordinary ergodic theory, based on infinite ergodic theory. Consider the energy of the system, which in the absence of interactions is purely kinetic. Usually, for normal gases this is  $k_B T/2$  per degree of freedom and one uses a perfectly normalized density to compute it, namely the Maxwell-Boltzmann

momentum distribution. Here, one needs to use a non-normalized state, with an important caveat: Only when the kinetic energy is integrable with respect to the non-normalizable state, is this strategy valid. This in turn means that observables like the energy of the system go through an ergodic transition as they switch from being integrable to non-integrable. The infinite density is not a description of far tails and its importance is found when the system is in the coldest state possible. This is vastly different from the Sisyphus system, since for sub-Doppler the anomalous statistics is found for shallow optical lattice, and far from ideal cooling scheme.

## VI. SUMMARY AND CONCLUSIONS

Theoretical advances in physics are often achieved when the existing theory fails to account for experimental observations. The advance of theoretical aspects of laser cooling was made possible due to surprisingly low temperatures found in the laboratory, which lead to the basic modelling and fundamental understanding of Sisyphus cooling. The predictions of this theory require modification when dealing with a fundamental transport property like the diffusion constant in the shallow lattice regime, signaling the breakdown of the canonical Green-Kubo relation and the emergence of super-diffusion. Similarly, the steady-state momentum distribution was found to yield infinite kinetic energy in the same regime. These challenges accentuated the need for the development of the tools surveyed in this Colloquium.

The main advantage of the system of laser-cooled atoms is its controllability, rarely found in experimental stochastic systems. A single experimental parameter, the depth of the optical lattice, controls the various dynamic phases of the system. The analysis of the scale-free process is made possible with a relatively simple tool, a Fokker-Planck equation, without invoking fractional derivatives or other ad-hoc assumptions. It was shown that the momentum distribution exhibits power-law statistics and a stable Lévy distribution describes the spatial spreading of the packet of particles. In particular, the concept of infinite density was employed to describe the far tails of the corresponding densities, allowing the accurate prediction of such basic quantities describing the process as the kinetic energy or the mean square displacement. Treated for many years by mathematicians as a pure abstract theory, this infinite ergodic theory is here linked to an actual physical system.

We presented experimental and theoretical evidence of the transition from Gaussian to Lévy spreading of the position of the atoms brought about by the peculiar, momentum-dependent force in the problem. We showed the breakdown of the steady-state solution and demonstrated how the confinement of the system yields deviations from Boltzmann-Gibbs equilibrium state. The dy-

namics of the position-momentum correlation function was also shown to be anomalous.

Fundamental concepts, rooted deeply in our understanding of statistical physics, are shown to be violated. Among those, we have established the need for a replacement of the Green-Kubo formalism, typically relating the diffusivity to a stationary correlation function, with one that takes into account the “ageing” of the correlation function in this system. This results in the ability to calculate transport constants previously predicted to be infinite.

Looking forward, we may speculate on the missing pieces of the puzzle. One aspect may be the effects of many-body physics on the anomalous statistics. How will atomic interactions drive the system to thermal equilibrium? Will this depend, and if so how, on the depth of the optical lattice? Another unexplored aspect of the problem relates to the Green-Kubo formalism. In transport theory, the relation between the response to a linear external weak field, namely the calculation of the mobility of the system, is a standard problem. Further exploration into this issue could serve a wider audience interested in anomalous response functions.

Experimentally, one can consider two frontiers: the first statistics-focused and the second single-particle-focused, each with its own advantages. The former is rooted in the fact that rare events and heavy tails require many decades of signal-to-noise to be resolved properly, whereas the latter is exciting in the sense that direct observations of paths can yield insights into the underlying processes that are washed out in the measurements of a large ensemble of particles. In particular, with single particle trajectories one can in principle analyse the time averages computed from long trajectories, and compare them to ensemble averages. This will promote a better understanding of the ergodic hypothesis in systems with scale-free dynamics. Modification of the external confining potential is also expected to lead to intricate behaviors which have yet to be explored. A third, crossover, regime is now slowly being made accessible through recent advances in the trapping of large arrays of single atoms (Morgado and Whitlock, 2021) and ions (Joshi *et al.*, 2021) combining single-particle control with relatively large statistics.

## VII. ACKNOWLEDGMENTS

The authors would like to thank Ariel Amir and Erez Aghion for their valuable input on the manuscript and Yoav Sagi, Andreas Dechant, Eric Lutz and Erez Aghion for important contributions to the work discussed in this Colloquium. The support of Israel Science Foundation’s grant 1898/17 is acknowledged (DK, EB).

## REFERENCES

- Aaronson, J. (1997), *An introduction to infinite ergodic theory*, 50 (American Mathematical Soc.).
- Afek, G., A. Cheplov, A. Courvoisier, and N. Davidson (2020), *Phys. Rev. A* **101**, 042123.
- Afek, G., J. Coslovsky, A. Courvoisier, O. Livneh, and N. Davidson (2017), *Phys. Rev. Lett.* **119**, 060602.
- Afek, G., and N. Davidson (2018), Unpublished.
- Agarwal, G., and K. Molmer (1993), *Phys. Rev. A* **47**, 5158.
- Aghion, E., D. A. Kessler, and E. Barkai (2017), *Phys. Rev. Lett.* **118**, 260601.
- Aghion, E., D. A. Kessler, and E. Barkai (2019), *Phys. Rev. Lett.* **122**, 010601.
- Agranov, T., P. Zilber, N. R. Smith, T. Admon, Y. Roichman, and B. Meerson (2020), *Phys. Rev. Research* **2**, 013174.
- Akimoto, T. (2008), *Journal of Statistical Physics* **132** (1), 171.
- Amir, A. (2020), *Thinking Probabilistically: Stochastic Processes, Disordered System, and Their Applications* (Cambridge University Press).
- Anderson, M., J. Ensher, M. Matthews, C. Wieman, and E. Cornell (1995), *Science* **269** (5221), 198.
- Ariel, G., A. Rabani, S. Benisty, J. D. Partridge, R. M. Harshey, and A. Be’er (2015), *Nature Communications* **6**, 8396.
- Aspect, A., E. Arimondo, R. Kaiser, N. Vansteenkiste, and C. Cohen-Tannoudji (1988), *Phys. Rev. Lett.* **61**, 826.
- Bar, A., Y. Kafri, and D. Mukamel (2007), *Phys. Rev. Lett.* **98** (3), 038103.
- Bar, A., Y. Kafri, and D. Mukamel (2008), *Journal of Physics: Condensed Matter* **21** (3), 034110.
- Bardou, F., J.-P. Bouchaud, A. Aspect, and C. Cohen-Tannoudji (2002), *Lévy statistics and laser cooling: how rare events bring atoms to rest* (Cambridge University Press).
- Bardou, F., J.-P. Bouchaud, O. Emile, A. Aspect, and C. Cohen-Tannoudji (1994), *Phys. Rev. Lett.* **72**, 203.
- Barkai, E., E. Aghion, and D. Kessler (2014), *Phys. Rev. X* **4** (2), 021036.
- Barkai, E., Y. Garini, and R. Metzler (2012), *Phys. Today* **65** (8), 29.
- Barkai, E., A. Naumov, Y. Vainer, M. Bauer, and L. Kador (2003), *Phys. Rev. Lett.* **91** (7), 075502.
- Barkai, E., G. Radons, and T. Akimoto (2021), *arXiv preprint arXiv:2104.03816*.
- Barkai, E., R. Silbey, and G. Zumofen (2000), *Phys. Rev. Lett.* **84** (23), 5339.
- Baudouin, Q., R. Pierrat, A. Eloy, E. J. Nunes-Pereira, P.-A. Cuniasse, N. Mercadier, and R. Kaiser (2014), *Phys. Rev. E* **90**, 052114.
- Bloembergen, N., E. Purcell, and R. Pound (1948), *Phys. Rev.* **73**, 679.
- Bouchaud, J.-P. (1992), *Journal de Physique I* **2** (9), 1705.
- Bouchaud, J.-P., and A. Georges (1990), *Physics Reports* **195** (4-5), 127.
- Bouganne, R., B. A. M., A. Ghermaoui, J. Beugnon, and F. Gerbier (2020), *Nature Physics* **16** (1), 21.
- Bouton, Q., J. Nettersheim, D. Adam, F. Schmidt, D. Mayer, T. Lausch, E. Tiemann, and A. Widera (2020), *Phys. Rev. X* **10**, 011018.
- Bray, A. (2000), *Phys. Rev. E* **62** (1), 103.



- Brokman, X., J. Hermier, G. Messin, P. Desbiolles, J.-P. Bouchaud, and M. Dahan (2003), *Phys. Rev. Lett.* **90**, 120601.
- Burnstein, A. (1981), *Chemical Physics Letters* **83** (2), 335.
- Burov, S., R. Metzler, and E. Barkai (2010), *Proceedings of the National Academy of Sciences* **107** (30), 13228.
- Castin, Y., J. Dalibard, and C. Cohen-Tannoudji (1991), Light Induced Kinetic Effects on Atoms, Ions, and Molecules, 5.
- Castin, Y., and K. Molmer (1990), *Journal of Physics B: Atomic, Molecular and Optical Physics* **23** (22), 4101.
- Chandrasekhar, S. (1943), *Reviews of modern physics* **15** (1), 1.
- Chistyakov, V. (1964), *Theory of Probability & Its Applications* **9** (4), 640.
- Chu, S. (1998), *Rev. Mod. Phys.* **70**, 685.
- Cohen-Tannoudji, C. (1998), *Rev. Mod. Phys.* **70**, 707.
- Cohen-Tannoudji, C., and D. Guéry-Odelin (2011), *Advances In Atomic Physics: An Overview* (World Scientific Publishing Company).
- Dalibard, J., and C. Cohen-Tannoudji (1985), *Journal of Physics B: Atomic and Molecular Physics* **18** (8), 1661.
- Dalibard, J., and C. Cohen-Tannoudji (1989), *J. Opt. Soc. Am. B* **6** (11), 2023.
- Dechant, A., D. A. Kessler, and E. Barkai (2015), *Phys. Rev. Lett.* **115**, 173006.
- Dechant, A., E. Lutz, E. Barkai, and D. Kessler (2011a), *Journal of Statistical Physics* **145** (6), 1524.
- Dechant, A., E. Lutz, D. Kessler, and E. Barkai (2011b), *Phys. Rev. Lett.* **107** (24), 240603.
- Dechant, A., E. Lutz, D. Kessler, and E. Barkai (2012), *Phys. Rev. E* **85** (5), 051124.
- Dechant, A., E. Lutz, D. Kessler, and E. Barkai (2014), *Phys. Rev. X* **4**, 011022.
- Dechant, A., S. T. Shafier, D. A. Kessler, and E. Barkai (2016), *Phys. Rev. E* **94**, 022151.
- Douglas, P., S. Bergamini, and F. Renzoni (2006), *Phys. Rev. Lett.* **96**, 110601.
- Duplat, J., S. Kheifets, T. Li, M. Raizen, and E. Villermaux (2013), *Phys. Rev. E* **87**, 020105.
- Einstein, A. (1905), *Annalen der physik* **17** (549-560), 208.
- Fogedby, H. C., and R. Metzler (2007a), *Phys. Rev. Lett.* **98**, 070601.
- Fogedby, H. C., and R. Metzler (2007b), *Phys. Rev. E* **76** (6), 061915.
- Gaunt, A. L., T. F. Schmidtz, I. Gotlibovych, R. P. Smith, and Z. Hadzibabic (2013), *Phys. Rev. Lett.* **110**, 200406.
- Gillespie, D. T., and E. Seitaridou (2012), *Simple Brownian diffusion: an introduction to the standard theoretical models* (Oxford University Press).
- Godreche, C., and J. Luck (2001), *Journal of Statistical Physics* **104** (3-4), 489.
- Green, M. S. (1954), *The Journal of Chemical Physics* **22** (3), 398.
- Hanke, A., and R. Metzler (2003), *Journal of Physics A: Mathematical and General* **36** (36), L473.
- Heshami, K., D. G. England, P. C. Humphreys, P. J. Bustard, V. M. Acosta, J. Nunn, and B. J. Sussman (2016), *Journal of Modern Optics* **63** (20), 2005, PMID: 27695198.
- Hirschberg, O., D. Mukamel, and G. M. Schütz (2011), *Phys. Rev. E* **84** (4), 041111.
- Hirschberg, O., D. Mukamel, and G. M. Schütz (2012), *Journal of Statistical Mechanics: Theory and Experiment* **2012** (02), P02001.
- Hodapp, T., C. Gerz, C. Furtlehner, C. Westbrook, W. D. Phillips, and J. Dalibard (1995), *Applied Physics B* **60** (2-3), 135.
- Holtzmark, J. (1919), *Annalen der Physik* **363** (7), 577.
- Holz, P. C., A. Dechant, and E. Lutz (2015), *Europhys. Lett.* **109** (2), 23001.
- Hänggi, P., and F. Marchesoni (2005), *Chaos: An Interdisciplinary Journal of Nonlinear Science* **15** (2), 026101.
- Jersblad, J., H. Ellmann, K. Stöckel, A. Kastberg, L. Sanchez-Palencia, and R. Kaiser (2004), *Phys. Rev. A* **69** (1), 013410.
- Joshi, M. K., F. Kranzl, A. Schuckert, I. Lovas, C. Maier, R. Blatt, M. Knap, and C. F. Roos (2021), “Observing emergent hydrodynamics in a long-range quantum magnet,” arXiv:2107.00033 [quant-ph].
- Kanazawa, K., T. Sano, A. Cairoli, and A. Baule (2020), *Nature* **579** (7799), 364.
- Kasevich, M., and S. Chu (1992), *Phys. Rev. Lett.* **69**, 1741.
- Kasevich, M., D. S. Weiss, E. Riis, K. Moler, S. Kasapi, and S. Chu (1991), *Phys. Rev. Lett.* **66**, 2297.
- Katori, H., S. Schlipf, and H. Walther (1997), *Phys. Rev. Lett.* **79** (12), 2221.
- Kessler, D. A., and E. Barkai (2010), *Phys. Rev. Lett.* **105** (12), 120602.
- Kessler, D. A., and E. Barkai (2012), *Phys. Rev. Lett.* **108** (23), 230602.
- Kindermann, F., A. Dechant, M. Hohmann, T. Lausch, D. Mayer, F. Schmidt, E. Lutz, and A. Widera (2016), *Nature Physics* **13**.
- Klauder, J., and P. Anderson (1962), *Physical Review* **125** (3), 912.
- Korabel, N., and E. Barkai (2009), *Phys. Rev. Lett.* **102** (5), 050601.
- Kubo, R. (1957), *Journal of the Physical Society of Japan* **12** (6), 570.
- Landau, L. D. (1944), *J. Phys.* **8**, 201.
- Levin, M., G. Bel, and Y. Roichman (2021), *The Journal of Chemical Physics* **154** (14), 144901.
- Levine, E., D. Mukamel, and G. M. Schütz (2005), *Europhys. Lett.* **70** (5), 565.
- Li, T., and M. G. Raizen (2013), *Annalen der Physik* **525** (4), 281.
- Livneh, O., G. Afek, and N. Davidson (2018), *Appl. Opt.* **57** (12), 3205.
- Lo, C.-C., L. Nunes Amaral, S. Havlin, P. Ivanov, T. Penzel, J.-H. Peter, and H. Stanley (2002), *Europhys. Lett.* **57** (5), 625.
- Ludlow, A. D., M. M. Boyd, J. Ye, E. Peik, and P. O. Schmidt (2015), *Rev. Mod. Phys.* **87**, 637.
- Lutz, E. (2003), *Phys. Rev. A* **67** (5), 051402.
- Lutz, E. (2004), *Phys. Rev. Lett.* **93**, 190602.
- Lutz, E., and F. Renzoni (2013), *Nature Physics* **9** (10), 615.
- Majumdar, S. (2007), in *The Legacy Of Albert Einstein: A Collection of Essays in Celebration of the Year of Physics* (World Scientific) pp. 93–129.
- Majumdar, S. N., and A. Comtet (2004), *Phys. Rev. Lett.* **92**, 225501.
- Majumdar, S. N., and A. Comtet (2005), *Journal of Statistical Physics* **119** (3), 777.
- Manning, G. S. (1969), *The Journal of Chemical Physics* **51** (3), 924.
- Margolin, G., and E. Barkai (2004), *The Journal of Chemical Physics* **121** (3), 1566.

- Margolin, G., and E. Barkai (2005), *Phys. Rev. Lett.* **94**, 080601.
- Margolin, G., V. Protasenko, M. Kuno, and E. Barkai (2006), *The Journal of Physical Chemistry B* **110** (38), 19053.
- Marksteiner, S., K. Ellinger, and P. Zoller (1996), *Phys. Rev. A* **53** (5), 3409.
- Martin, E., U. Behn, and G. Germano (2011), *Phys. Rev. E* **83**, 051115.
- Mayer, D., E. Lutz, and A. Widera (2020), *arXiv preprint arXiv:2005.04059*.
- Mercadier, N., W. Guerin, M. Chevrollier, and R. Kaiser (2009), *Nature Physics* **5** (8), 602.
- Metzler, R., J.-H. Jeon, A. G. Cherstvy, and E. Barkai (2014), *Physical Chemistry Chemical Physics* **16** (44), 24128.
- Metzler, R., and J. Klafter (2000), *Physics Reports* **339** (1), 1.
- Miccichè, S. (2010), *Europhys. Lett.* **92** (5), 50011.
- Milburn, G. J. (1988), *J. Opt. Soc. Am. B* **5** (6), 1317.
- Morgado, M., and S. Whitlock (2021), *AVS Quantum Science* **3** (2), 023501.
- Mulder, R. A., M. A. Caracanhas, and C. M. Smith (2021), *Phys. Rev. B* **103**, 174301.
- Phillips, W. D. (1998), *Rev. Mod. Phys.* **70**, 721.
- Plerou, V., P. Gopikrishnan, L. A. Nunes Amaral, X. Gabaix, and S. H. Eugene (2000), *Phys. Rev. E* **62**, R3023.
- Poland, D., and H. A. Scheraga (1966), *The Journal of Chemical Physics* **45** (5), 1456.
- Poletti, D., P. Barmettler, A. Georges, and C. Kollath (2013), *Phys. Rev. Lett.* **111**, 195301.
- Poletti, D., J.-S. Bernier, A. Georges, and C. Kollath (2012), *Phys. Rev. Lett.* **109**, 045302.
- Redner, S. (2001), *A guide to first-passage processes* (Cambridge University Press).
- Reichel, J., F. Bardou, M. B. Dahan, E. Peik, S. Rand, C. Salomon, and C. Cohen-Tannoudji (1995), *Phys. Rev. Lett.* **75**, 4575.
- Richardson, L. (1926), *Proceedings of the Royal Society of London. Series A, Containing Papers of a Mathematical and Physical Character* **110** (756), 709.
- Romer, R., and R. Dicke (1955), *Phys. Rev.* **99**, 532.
- Sagi, Y., I. Almog, and N. Davidson (2010), *Phys. Rev. Lett.* **105**, 093001.
- Sagi, Y., M. Brook, I. Almog, and N. Davidson (2012), *Phys. Rev. Lett.* **108** (9), 093002.
- Sagi, Y., R. Pugatch, I. Almog, N. Davidson, and M. Aizenman (2011), *Phys. Rev. A* **83**, 043821.
- Saubamea, B., M. Leduc, and C. Cohen-Tannoudji (1999), *Phys. Rev. Lett.* **83** (19), 3796.
- Shlesinger, M. F., B. J. West, and J. Klafter (1987), *Phys. Rev. Lett.* **58**, 1100.
- Stefani, F. D., J. Hoogenboom, and E. Barkai (2009), *Phys. Today* **62** (2), 34.
- Stoneham, A. (1969), *Reviews of Modern Physics* **41** (1), 82.
- Taylor, G. I. (1922), *Proceedings of the London Mathematical Society* **2** (1), 196.
- Vezzani, A., E. Barkai, and R. Burioni (2019), *Phys. Rev. E* **100** (1), 012108.
- Wickenbrock, A., P. C. Holz, N. A. A. Wahab, P. Phoonthong, D. Cubero, and F. Renzoni (2012), *Phys. Rev. Lett.* **108**, 020603.
- Wineland, D. J., R. E. Drullinger, and F. L. Walls (1978), *Phys. Rev. Lett.* **40**, 1639.
- Zaburdaev, V., S. Denisov, and J. Klafter (2015), *Rev. Mod. Phys.* **87**, 483.